scientific reports

Check for updates

OPEN

The novel amino-artemisinin derivative WHN-11 disrupts mitochondria and protein homeostasis, and induces autophagy and apoptosis in cancer cells

Deborah Kajewole[1,2], Ho Ning Wong[3], Alexander von Kriegsheim[4], Richard K. Haynes[3,5], Jo-Anne de la Mare[1] & Adrienne Lesley Edkins[1]✉

Semi-synthetic derivatives of artemisinin exhibit anti-cancer activity in vitro and in vivo in addition to anti-malarial activity. Here, we report the anti-cancer and anti-cancer stem cell potential of novel C-10 substituted amino-artemisinin derivatives. Of these, the 4′-trifluoromethylarylurea piperazinyl derivative WHN-11 demonstrated cytotoxic activity at high nanomolar concentrations across a range of cancer cell lines. WHN-11 reduced short- and long-term survival of triple-negative breast cancer (TNBC) cells, a highly aggressive breast cancer subtype that currently lacks standardized targeted treatments. Mechanistically, WHN-11 induced a stress response and increased proteasome-mediated turnover of ubiquitinated proteins. WHN-11 promoted mitochondrial depolarization and fission, suppressing the expression of anti-apoptotic B-cell lymphoma extra-large (Bcl-xL) protein and ATP synthesis, thereby decreasing cellular energy production, and inducing apoptosis. WHN-11 treatment also increased autophagosomes, acidic vesicular organelles and lipid droplets. Activation or inhibition of autophagy synergized with the activity of WHN-11 in promoting cellular toxicity, as did increasing cellular dependence on oxidative phosphorylation. Unexpectedly, the effects of WHN-11 appear independent of substantial reactive oxygen species (ROS) production. Taken together, these data suggest that amino-artemisinins related to WHN-11 are promising candidates for anti-TNBC therapies targeting the mitochondria alone or in combination with autophagy modulators.

Keywords Amino-artemisinin, Triple-negative breast cancer (TNBC), Reactive oxygen species (ROS), Apoptosis, Autophagy, Mitochondrial fission

The antimalarial drug artemisinin is the active component of the sweet wormwood *Artemisia annua* that has long been used in Traditional Chinese Medicine for its antipyretic properties[1]. Artemisinin and its synthetic derivatives (Fig. 1) are promising candidates for repurposing for other conditions such as autoimmune diseases and inflammation[2–5], other parasitic infections[6], viral infections[6–9] and cancer[10]. Artemisinins are active against cancer cells in vitro and against tumours in vivo[11–18]. Artesunate has been submitted to clinical trials[19,20] although regression-free survival was not enhanced. Against tumour cells in vitro, the amino-artemisinin artemisone elicits activities superior to artemisinin[21]. In principle, because of relative lack of toxicity and enhanced pharmacokinetic properties including lack of metabolism to DHA, artemisone is better suited for clinical use[22]. IC_{50} activities of artemisinins in vitro range from 0.26 to 95.7 µM against a variety of tumour cell lines[19,20,23–25]. Combinations of artemisinins with known and developmental cancer drugs have been examined,

[1]Biomedical Biotechnology Research Unit (BioBRU), Department of Biochemistry, Microbiology and Bioinformatics, Rhodes University, Makhanda 6139, South Africa. [2]Huntsman Cancer Institute, University of Utah, Salt Lake City, USA. [3]Rural Health Research Institute, Charles Sturt University, Orange, NSW 2800, Australia. [4]Institute of Genetics and Cancer, University of Edinburgh, Edinburgh, Scotland, UK. [5]Centre of Excellence for Pharmaceutical Sciences, Faculty of Health Sciences, North-West University, Potchefstroom 2531, South Africa. ✉email: a.edkins@ru.ac.za

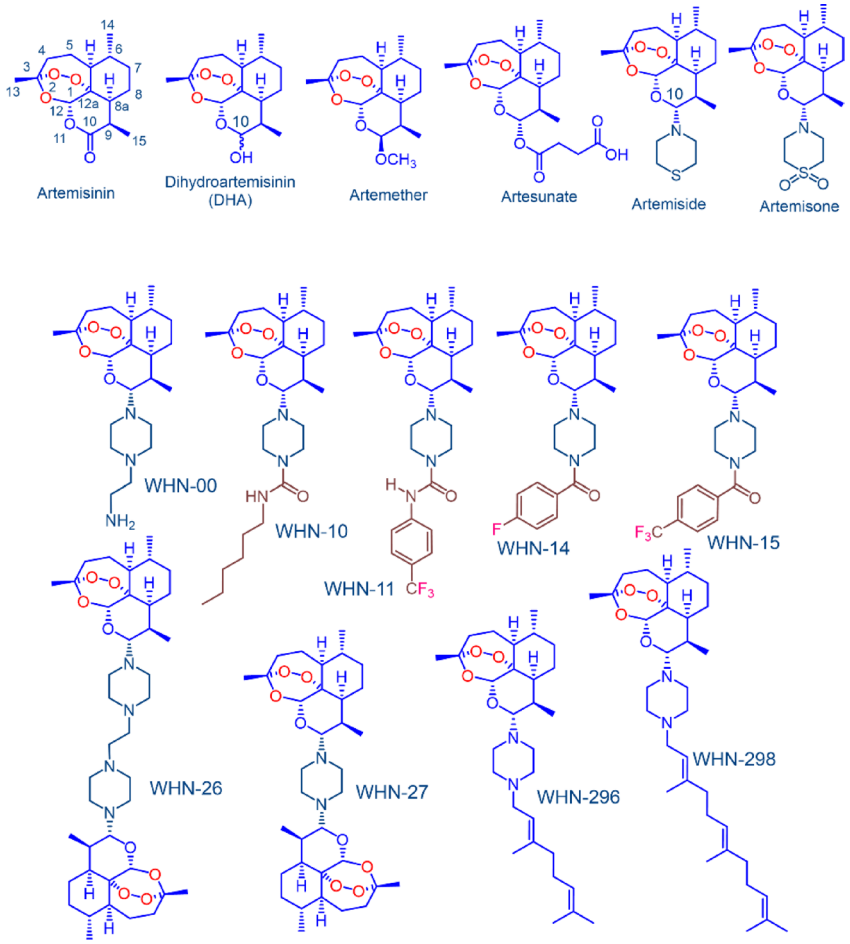

Fig. 1. Current clinical artemisinin derivatives and the novel amino-artemisinins. The current clinical derivatives are used for treatment of malaria. Artemether and artesunate are rapidly converted into DHA in vivo via facile metabolism or hydrolysis, respectively. The amino-artemisinins artemiside and artemisone differ in possessing a nitrogen atom at C-10 that enhances biological activities, and are not metabolized to DHA, an important feature for selection of amino-artemisinins for drug development campaigns targeting diseases other than malaria. The piperazinyl ureas, WHN-10 and WHN-11, the piperazinyl amides, WHN-14 and WHN-15[47], the DHA-piperazine dimer WHN-27[19], the geranyl- and farnesyl-piperazine derivatives WHN-296 and WHN-298[20] have been prepared previously. The aminoethyl¬piperazine derivative WHN-00 and the dimer WHN-26 are reported here for the first time; details of their preparation and spectroscopic data are given in the Supplementary files.

largely with the view of enhancing activity of the latter through additivity or synergism. This would attenuate toxicity of the partner drug through use of lower amounts[26,27]. In this respect, artemisone shows additivity in its combinations with oxaliplatin and gemcitabine[21]. Activity of artemisone (IC_{50} 95.7 μM) towards A375 melanoma cells is synergized in combination with the redox-active copper-(II) complex of the anti-cancer drug elesclomol[28]. The geranyl and farnesyl piperazine derivative WHN-296 and WHN-298 likewise act in synergy with the elesclomol-copper(II) complex against A375 melanoma cells[28].

The antitumour action of artemisinins are pleiotropic. Artemisinins increase oxidative stress through generation of reactive oxygen species (ROS) that induce downstream signalling effects to overwhelm redox homeostasis in the cancer cell, and induce cell-cycle arrest and apoptosis[21,25,29–32]. One potential pathway involves oxidation by the artemisinin of reduced flavin cofactors of disulfide reductases such as glutathione reductase (GR), thioredoxin reductase (TrxR) and others[32–34]. ROS is produced during treatment of A375 melanoma cells with the geranyl piperazine derivative WHN-296[28]. There is pronounced synergism of amino-artemisinins with the redox active elesclomol-copper(II) complex, which is known to exert activity by generation of ROS[35]. However, mechanistic pathways independent of ROS generation have also been reported[36,37].

Here, we report the anti-cancer activities of a distinct class of artemisinin derivatives termed amino-artemisinins (Fig. 1) against cancer cell lines including triple-negative breast cancer (TNBC) cells. TNBCs make up 15–20% of reported breast cancer cases, are highly aggressive, and lack effective standardised chemotherapeutic treatment regimens[38–42]. Amino-artemisinins, obtained from DHA by replacing the hydroxyl group at C-10 by an amino group (Fig. 1)[43,44], have greatly enhanced efficacies against the malaria parasite and cancer cells[28,45–48]. These derivatives have improved pharmaco kinetics[13], and generate active metabolites with relatively long half-

lives[47]. Using established artemisinins (Fig. 1) as controls, we identify the 4'-trifluoromethylarylurea piperazinyl derivative WHN-11 as an anti-cancer hit compound, with a mechanism of action targeting the mitochondria to induce autophagy and apoptosis independent of explicit ROS generation.

Materials and methods

Compounds

Reference compounds and the artemisinins used for screening were ≥ 95% pure as established previously[28,45,46]. The piperazinyl ureas WHN-10 and WHN-11, the piperazinyl amides WHN-14 and WHN-15[47] and the DHA-piperazine dimer WHN-27[48] were prepared and characterized as reported previously. Elesclomol, 98% pure, was obtained from Kaixuan Chemical Company, Changzhou, Jiangsu, China, and used as received[28]. For screening as described below, compounds were dissolved in dimethyl sulfoxide (DMSO) to a stock concentration of 100 mM and stored at – 20 °C.

Cell cultures

The triple negative breast cancer cell lines HCC1937 (ATCC: CRL-2336), HCC70 (ATCC: CRL-2315), MDA-MB-231 (ATCC: HTB-26), the cervical carcinoma cell line HeLa (ATCC: CCL-2), and colon cancer cell line HCT116 (ATCC: CCL-247) were purchased from the ATCC. The glioblastoma U-87 (ATCC: HTB-14), 501mel melanoma (CVCL_4633) and HEK293T (ATCC: CRL-3216) cell lines were provided by Prof. Sharon Prince, Department of Human Biology, University of Cape Town, South Africa, and the MCF-12A (ATCC: CRL-10782) breast epithelial cell line was provided by Prof. Anna-Mart Engelbrecht, Department of Physiological Sciences, Stellenbosch University, South Africa. The culture conditions are reported in Supplementary Table 1. All cell lines were cultured at 37 °C and 9% CO_2 and were confirmed to be mycoplasma-free by Hoechst 33,342 staining. Cells used for experiments were between 10 and 30 passages.

Viability assay using *3-(4,5-dimethylthiazol-2-yl)-2,5-diphenyl-2H-tetrazolium bromide* (MTT) dye

For all cell lines other than the MDA-MB-231-line, viability was assessed based on the conversion of MTT dye into the insoluble formazan. Cells seeded overnight in 96-well plates (5×10^3 cells/well) were treated for 72 h with increasing concentrations of the compounds or 0.1% (v/v) DMSO in culture medium. Thereafter, cells were incubated with 200 µg/mL MTT dye for 4 h and an insoluble formazan was produced overnight with 10% (w/v) acidified SDS solution. Absorbance was measured at 595 nm and the half maximal inhibitory concentrations (IC_{50}) of the compounds were calculated by non-linear regression using GraphPad Prism version 4.00 (San Diego, CA, USA).

Viability assay using sulforhodamine B (SRB) dye

For the cytotoxicity screening with the MDA-MB-231 cell line, SRB dye was used since the MTT assay gave poor results for this cell line. Cells seeded in 96-well plates (1×10^4 cells/well) overnight were treated as per the MTT assay. Subsequently, cells were fixed with cold 50% (w/v) aqueous trichloroacetic acid (TCA) for an hour at 4 °C, washed in slow-running water and the plate air-dried. Fixed cells were stained with 0.04% (w/v) SRB in acetic acid for an hour, washed repeatedly with 1% (v/v) aqueous acetic acid to remove unbound dye and solubilized for 10 min with 10 mM Tris base solution (pH 10.5) on an orbital shaker. Absorbance was measured at 510 nm and the IC_{50} values determined as described above.

Tumoursphere assay for cancer stem cell activity

As previously described[49], HCC1937 cells were seeded as single cell suspensions into a 96-well Corning® Costar® Ultra-Low attachment multiple well plate (1×10^3 cells/well). Cultures were grown in anchorage-independent growth (AIG) medium consisting of DMEM supplemented with 1% (v/v) PSA, 2% (v/v) B-27 supplement, 1% (v/v) GlutaMAX, 20 ng/mL human epidermal growth factor (hEGF), 20 ng/mL basic fibroblast growth factor (bFGF), 4 ng/mL heparin and 10 µg/mL insulin. Cells were immediately treated with 0.1% (v/v) DMSO or 50 µM of each compound and incubated for 7 days. Treated cells were supplemented with freshly prepared AIG medium at 48-h intervals. Tumourspheres formed were quantified at the end of the incubation period to calculate the percentage Tumoursphere Forming Efficiency (TFE): (average total number of tumoursphere formed/number of cells seeded) × 100%.

Clonogenic assay in treated HCC1937 cells

Seeded cells (1.5×10^2 cells/well) were incubated for 6 h, treated with 0.1% (v/v) DMSO, 5-fluorouracil (5-FU) or WHN-11 for 9 days and supplemented with fresh complete medium every 2 days. Colonies were fixed with methanol:acetic acid (3:1) and stained overnight with 1% (w/v) crystal violet in methanol. Excess stain was removed in slow-running water and the plate air-dried. Pictures of colonies were taken using a Molecular Imager ChemiDoc XRS + System (Bio-Rad, USA). To quantify the colonies formed, crystal violet-stained cells were solubilized with 1% (w/v) acidified-SDS for 4 h at 37 °C and absorbance measured at 570 nm.

SDS-PAGE and western blot analysis

According to the standard modifications of the Laemmli protocol[50], equal amounts of protein from treated whole cell lysates were resolved on a 12% SDS-PAGE gel and transferred to nitrocellulose membrane. Membranes were blocked for 1 h in 1% (w/v) Tris-buffered saline (TBS) containing 1% (w/v) solution of non-fat powdered milk (Blotto). Thereafter, membranes were incubated overnight with specific primary antibodies in 0.1% (v/v) TBS-Tween-20 (TBST) containing 1% (w/v) Blotto at 4 °C. Membranes were submitted to repeated washes with 0.1% TBST, prior to incubation with secondary antibodies and protein bands visualized by chemiluminescence using

Clarity Western Enhanced chemiluminescence (ECL) substrate (Bio-Rad; 170–5061) on a Molecular Imager ChemiDoc XRS + System (Bio-Rad, USA).

Proteomic analysis of differentially expressed genes in WHN-11 treated HCC1937 cells by mass spectrometry

HCC1937 cells treated with 0.1% (v/v) DMSO or 10 µM WHN-11 were harvested and lysed in PBS buffer (pH 7.4) containing 0.1% (v/v) Triton-X100 and 1 mM phenylmethansulfonyl fluoride (PMSF). Equal amounts of protein (~ 50 µg) were resuspended at a 5:1 ratio in digestion solution containing 5% (w/v) sodium deoxycholate (Sigma-Aldrich; D6750), 50 mM tris-(2-carboxyethyl)phosphine, hydrochloride (TCEP-HCl, Thermo Fisher Scientific; 20,490) and 100 mM chloroacetamide (Sigma-Aldrich; C0267) for 5 min at 95 °C. Lysates were digested at a 100:1 ratio with mass spectrometry (MS)-grade trypsin protease (Thermo Fisher Scientific; 90,057) at 37 °C overnight. Digested samples were incubated with 5% (v/v) trifluoroacetic acid (TFA, Thermo Fisher Scientific; 85,183) in isopropanol and centrifuged at 12,000 × g for 10 min at 4 °C. The supernatants were transferred to styrene divinylbenzene polymer (SDB) spin-columns and centrifuged at 1,000 × g for 5 min. Samples were first washed with isopropanol containing 1% (v/v) TFA and then with 0.2% (v/v) TFA in MS grade water. Mass spectra were collected and analysed on a Q-Exactive MS connected to an Ultimate Ultra 3000 chromatography system (Thermo Scientific, Germany) as previously described[51]. Gene set enrichment analysis (GSEA) using the c5.all.v7.5.1.symbols.gmt [Gene Ontology] gene sets database was conducted on the genes in the proteomic dataset comparing WHN-11 treated lysates to a DMSO-treated control. A thousand permutations were run, and the maximum and minimum gene set sizes set to 500 and 15, respectively[52,53].

Indirect immunofluorescence staining for the detection of ubiquitinated proteins

Cells grown on sterile coverslips (1×10^5 cells/well) were treated overnight with 0.1% (v/v) DMSO in culture medium or 10—50 µM WHN-11. Thereafter, cells were fixed briefly with ice-cold methanol and permeabilised with 0.1% (v/v) Triton-X100, blocked with 1% (w/v) bovine serum albumin (BSA) containing 1X TBS and incubated overnight with anti-ubiquitin antibody (Santa Cruz; sc-8017) at 4 °C. Following incubation with Alexa-Fluor 488 anti-mouse secondary antibody (Abcam; ab15105) and Hoechst 33,342, coverslips were mounted on slides with DAKO fluorescence mounting medium (DAKO; S3023). Images were captured using laser wavelengths of Ex_{488nm}/Em_{562nm} on a Zeiss LSM 780 confocal microscope and analysed using Zeiss Zen 2 (blue edition) software, version 2.0 (Carl Zeiss Microscopy, GmbH).

Chymotrypsin-like proteasome activity assay

Cell pellets were lysed in proteasome lysis buffer (50 mM HEPES pH 7.8, 10 mM NaCl, 1.5 mM $MgCl_2$, 1 mM EDTA, 1 mM EGTA, 250 mM sucrose and 5 mM DTT) for 20 min at 4 °C. Lysates were sonicated, cleared by centrifugation, the supernatant collected, and equal amounts of protein (~ 16 µg) seeded into black-walled 96-well plates for proteasome assay. Lysate was incubated with compounds or DMSO control for an hour at 37 °C in proteasome lysis buffer containing 2 mM ATP and 100 µM of *N*-succinyl-Leu-Leu-Val-Tyr-7-amido-4-methyl-coumarin proteasome substrate (Suc-LLVY-AMC, Sigma-Aldrich; S6510). Fluorescence was measured at Ex_{360nm}/Em_{460nm} and the proteasome activity of each treatment was determined relative to the vehicle control.

Analysis of caspase activation for the detection of apoptosis

HCC1937 cells (5×10^5 cells/well) seeded overnight were treated for 24 h with 0.1% (v/v) DMSO, 5 µM KRIBB-11 or 1—50 µM WHN-11. Using Vybrant™ FAM poly caspases assay kit (Thermo Fisher Scientific, V35117), cells were pelleted, incubated in the dark at 37 °C, 9% CO_2 with 1X FLICA reagent for an hour and briefly stained with 1.25 µg/mL propidium iodide. Fluorescence was detected on a BD FACSAria II flow cytometer (BD Biosciences, San Jose, CA, USA) using Ex_{488nm} and Em_{530nm} filters, and analysed with FlowJo v10.0.7 software (FlowJo, LLC).

Identification of acidic vesicular organelles (AVOs) using acridine orange staining

Cells were seeded (2×10^4 cells /well) in a 15µ-slide angiogenesis chamber (Ibidi GmbH, 81,506) and treated for 4 h with compounds. Live cells were briefly stained in the dark with 1 µg/mL Acridine Orange hemi (zinc chloride) salt (Sigma-Aldrich, A6014). Excess stain was removed by washing with PBS (pH 7.4) and coverslips mounted on slides with DAKO mounting medium. Images were captured using laser wavelengths of Ex_{561nm}/Em_{637nm} for red signals and Ex_{488nm}/Em_{539nm} for green signals on a Zeiss LSM 780 confocal microscope as described above.

Nile red staining for lipid droplets

Cells seeded in 15µ-slide angiogenesis chambers (Ibidi GmbH) were treated for 4 h with compounds. Thereafter, cells were washed once with HBSS containing 20 mM HEPES pH 7.0 (HHBS). Live cells were stained in the dark for 30 min with 200 nM Nile Red dye in HHBS at room temperature. Excess stain was removed by washing with 1X HHBS and cells were mounted on slides with DAKO mounting medium. Images were captured for differential interference contrast (DIC) or Nile Red signals using laser wavelengths of Ex_{488nm}/Em_{566nm} on a Zeiss LSM 780 confocal microscope as described above.

Direct immunostaining for Bcl-xL protein expression

Treated HCC1937 cells were harvested, fixed with 0.01% (v/v) formaldehyde in PBS, and resuspended in permeabilization (PERM) buffer containing 0.1% (v/v) Triton-X100 and 0.5% (w/v) BSA in PBS (pH 7.4) in the dark for 15 min. Cells were pelleted and subjected to immunostaining with PERM buffer containing 1 µg of mouse PE-conjugated IgG1 Kappa isotype control (eBiosciences, 12–4714-42) or PE-conjugated anti-Bcl-xL (H-5) antibody (Santa Cruz, sc-8392) for an hour at 4 °C. Fluorescence was detected using a BD FACSAria II

flow cytometer (BD Biosciences, San Jose, CA, USA) using laser wavelengths of Ex_{480nm}/Em_{575nm} to determine the expression of Bcl-xL protein, represented as the mean fluorescence intensity (MFI).

Detection of cellular ATP concentrations
ATP levels in treated HCC1937 cells was assessed using the ATP Bioluminescence Assay Kit CLS II (Roche, 11–699-695–001). Cells were lysed at 4 °C for 10 min in lysis buffer containing 50 mM Tris buffer, 5% (v/v) glycerol, 1 mM DTT, 60 mM $MgCl_2$ and 150 mM NaCl. ATP concentrations between 50 pM and 50 µM were used as standards. Equal volumes of lysate or standard samples and luciferase reagent were mixed in a 96-well plate and luminescence was measured.

JC-1 staining for mitochondrial membrane potential
Treated HCC1937 cells were stained with 2.5 µg/mL JC-1 dye (Abcam; ab113850) for 30 min as previously described[54]. Harvested cells were thereafter analysed on a BD FACSAria II flow cytometer (BD Biosciences, San Jose, CA, USA). For each sample, 10,000 events were recorded using Ex_{488nm}/Em_{529nm} and Ex_{488nm}/Em_{590nm} for green and red signals, respectively. Carbonyl cyanide *m*-chlorophenyl hydrazone (CCCP) treatment was used as a control for loss of mitochondrial membrane potential.

Colocalization of TRAP1 with Bcl-xL in treated cells
HCC1937 cells treated for 3 h were fixed with 4% (w/v) aqueous PFA, permeabilised and incubated for an hour with 1% (w/v) BSA in 1X TBS. Following this, cells were incubated at 4 °C overnight with primary anti-TRAP1 antibody (Thermo Fisher; MA1-010) in 0.1% BSA-TBST buffer (1:100) and for an hour with Alexa-Fluor 488 secondary anti-mouse antibody (Abcam; ab15105) in the dark. Stained cells were also incubated for 1.5 h with 1 µg of PE-conjugated Bcl-xL (H-5) antibody (Santa Cruz; sc-8392) and Hoechst 33,342 at 4 °C and mounted on slides with DAKO mounting medium. Images were captured using laser wavelengths of Ex_{488nm}/Em_{557nm} for Alexa-Fluor 488 signals and Ex_{561nm}/Em_{618nm} for PE signals on a Zeiss LSM 780 confocal microscope as described above.

Cell survival assay for galactose-dependent mitochondrial function
HCC1937 cells were seeded either in glucose-containing medium (as in the MTT assay) or in galactose-containing medium [RPMI-1640 (Thermo Fisher Scientific; 11,879,020) supplemented with 2 g/L galactose, 10% (v/v) FBS, 1% (v/v) 100 U/mL PSA, 1% (v/v) GlutaMAX™ and 0.25% (v/v) sodium bicarbonate]. Thereafter, cells were treated with compounds and processed as previously described with the MTT assay to determine the IC_{50} values.

Immunoprecipitation of Bcl2 proteins in treated HEK293T cells
HEK293T cells were transiently co-transfected with 2 µg of purified pLV-eGFP (control; Addgene plasmid 36,083) and 2 µg GFP-Bcl2 (Addgene plasmid 17,999) or Beclin1-FLAG (Addgene plasmid 24,388) for 48 h. Thereafter, cells were treated for 3 h with 0.1% (v/v) DMSO, HBSS, 5 µM colchicine or 20 µM WHN-11. Equal amount of protein from harvested lysate was incubated overnight at 4 °C with 5 µg/mL magnetic anti-GFP conjugated beads (Abcam; ab193983). GFP-bound protein complexes were eluted and resolved on a 12% SDS-PAGE gel and subject to immunoblot analysis for GFP-Bcl2 and Beclin1 (FL) using anti-GFP and anti-FLAG antibodies, respectively. Densitometry analysis was conducted using ImageJ 1.51j8 NIH freeware.

Combination assay for the analysis of synergistic relationships between compounds
Using the standard compound combination protocols[36,37,55], HCC1937 cells were treated at constant or non-constant ratios with the relevant compounds for 72 h and subjected to MTT assay as previously described. Combination indexes (CI) were developed from constant ratio of combined compounds and algorithms in CompuSyn software, version 1.0 as previously described[56]. CI was defined as synergistic ($CI < 1$), additive ($CI = 1$) or antagonistic ($CI > 1$) from a graph representing the CI versus Fa (fraction of cells affected).

Statistical analysis
All quantitative data were analyzed to assess statistical significance using GraphPad Prism. For comparisons between multiple groups, One- or Two-way analysis of variance (ANOVA) was performed, followed by post-hoc testing with appropriate multiple comparison tests, to determine pairwise differences. Otherwise, a student's t-test was applied for comparison between two groups. The specific statistical significance cutoffs applied are outlined in respective figure legends.

Results

Amino-artemisinin derivatives exhibit anti-cancer and anti-cancer stem cell activity in vitro: selection of WHN-11 as hit compound.

To expand the amino-artemisinin repertoire, we used our synthetic methodologies originally developed for preparing artemiside and artemisone from DHA[45,57]. This led to production of the C-10 substituted piperazinyl derivatives (Fig. 1)[28,47,48]. Details on preparation of these compounds are provided in the supplementary data.

We established the half-maximal inhibitory concentrations (IC_{50}) of artemisinins against HCC1937, HCC70 and MDA-MB-231 TNBC cell lines, HeLa cervical carcinoma, U87 glioblastoma, 501mel melanoma and HCT116 colon cancer cell lines, as well as the non-cancerous non-transformed breast epithelial MCF-12A and human embryonic kidney HEK293T cell lines (Fig. 2a; Supplementary Table 2). The amino-artemisinins exhibited increased toxicity against all cell lines compared to the parent compound artemisinin (Fig. 2a; Supplementary Table 2). Consistent with previous studies, DHA and artesunate showed greater toxicities against

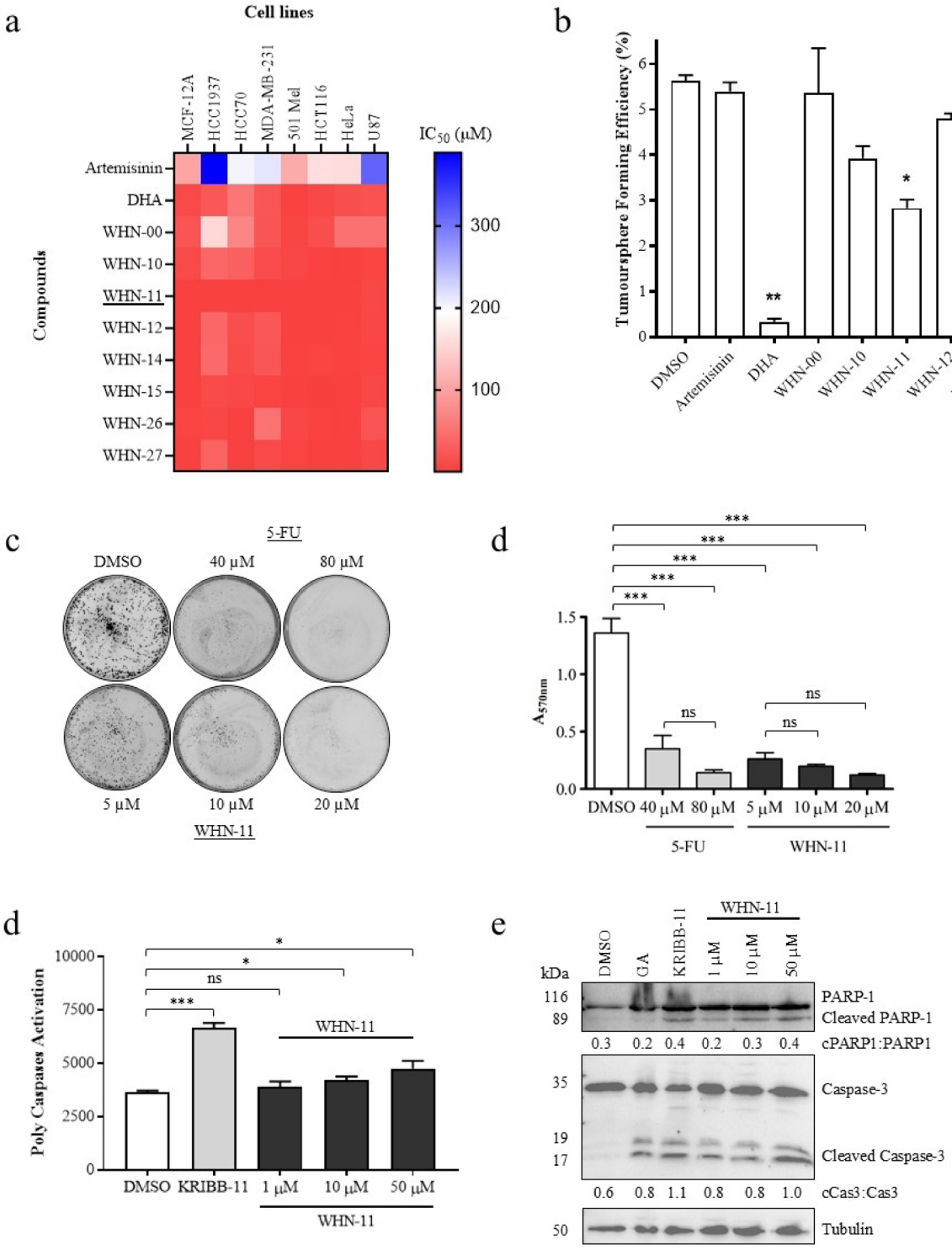

all cell lines compared to artemisinin (Supplementary Table 2)[58]. Notably, compared to artemisinin, the WHN-series of amino-artemisinins had IC_{50} values in the low micromolar/high nanomolar range across all cell lines. WHN-11 was consistently the most toxic in all cell lines tested (Fig. 2a, Supplementary Table 2). WHN-11 was substantially more toxic to all cancer cell lines except the U87 glioblastoma compared to the HEK293T cell line (SI values from 2.85–12.58; Supplementary Table 2).

We next investigated the ability of artemisinins to inhibit cancer stem-like cell (CSC) activity. The ability of CSCs to both self-renew and differentiate is linked to metastases and chemoresistance[59,60]. This was assessed in vitro through the formation of tumourspheres, which grow anchorage independently in serum-free, non-adherent growth conditions. CSC are enriched in $CD44^{+}/CD24^{-}$ stem-like cells, which express higher levels of the Oct4 stem cell transcription factor[49]. DHA, artesunate, WHN-11 and WHN-298 inhibited tumoursphere formation in the HCC1937 TNBC cell line (Fig. 2b). Given its potent cytotoxicity across both cancerous and

◀**Fig. 2**. Novel artemisinin derivatives exhibit anti-cancer and anti-cancer stem cell activity (**a**) Heatmap showing the IC_{50} values (in μM) of artemisinins screened against non-cancerous MCF-12A epithelial breast cell line, TNBC cell lines: HCC1937, HCC70, MDA-MB-231; non-breast cancer cell lines: 501 melanoma, HCT116, HeLa and U87 cell lines. DHA – dihydroartemisinin (**b**) Percentage tumoursphere forming efficiency (%TFE) of cells cultured in AIG media and treated at a single-point concentration of each compound (50 μM) or DMSO for 7 days; % TFE = [total number of tumoursphere formed / number of cells seeded] × 100%. Data shown as averages ± SEM (n = 3) and statistical significance were determined using one-way ANOVA with Bonferroni's multiple comparisons test. Significance levels relative to DMSO-treatment are indicated as * $p < 0.05$, ** $p < 0.01$. (**c**) Representative images of colonies formed in a clonogenic assay for treated HCC1937 cells cultured over 9 days. Following solubilization, average absorbance at 570 nm (A_{570nm}) ± SEM (n = 3) was measured. Statistical significance was assessed by one-way ANOVA with Tukey's multiple comparison test, where significance levels are indicated as *** $p < 0.001$ and ns—not significant. 5FU: 5-fluorouracil (**d**) Caspase activation in treated HCC1937 cells using Vybrant™ FAM Poly Caspase Assay Kit. Data shown are MFI average ± SEM (n = 3), where significance levels are indicated as * $p < 0.05$, *** $p < 0.001$ and ns—not significant using a two-tailed student's t-test analysis. (**e**) Western blot analysis of PARP-1 and Caspase-3 activation in treated cells, tubulin was used as a loading control. GA: geldanamycin (see Supplementary blot figure F1 for full length blots).

normal cell lines, WHN-11 was considered for further evaluation. Despite its lack of selectivity for cancer cells, we sought to investigate its potential in anti-cancer therapy by deciphering its underlying mechanism of action.

We next examined the ability of WHN-11 to block long-term cell survival using the clonogenic assay[61]. Both 5-fluorouracil (5-FU), which impairs DNA synthesis, apoptosis and therefore colony formation[62], and WHN-11 significantly decreased colony formation of HCC1937 cells in a dose-dependent manner (Fig. 2c). WHN-11 c increased activation of caspases in HCC1937 cells indicating that the WHN-11 effect was cytotoxic and not cytostatic (Fig. 2d). Similar to geldanamycin (GA) and KRIBB-11, WHN-11 promoted the cleavage of caspase-3 [but not poly-ADP ribose polymerase-1 (PARP-1)] in a dose-dependent fashion (Fig. 2e). This indicated that WHN-11 induced apoptosis. KRIBB-11 and GA, known modulators of the cellular stress response (CSR)[63,64], were included as controls to confirm apoptosis[65,66]. Both controls showed increased caspase-3 cleavage, providing a basis for comparison with WHN-11. Notably, artemisinins often exert activity through reactive oxygen species (ROS) generation, disrupting homeostasis and inducing cell-cycle arrest and apoptosis[20,21,29,32,38–41]. Therefore, to identify and quantitate ROS production in HCC1937 cells treated with WHN-11, we used 2',7'-dichlorodihydrofluorescein diacetate (DCFDA). DCFDA has been used previously to demonstrate ROS production by artemisinins[20,67]. H_2O_2 and artemisinin significantly induced ROS formation, but WHN-11 did not induce significant levels of ROS compared to the vehicle treatment (Supplementary Fig. 1a). We next used an alternative assay that links ROS detection to the activation of an antioxidant response element (ARE) reporter plasmid based on the NADP(H):quinone oxidoreductase 1 (NQO1) promoter[68].the NADP(H):quinone oxidoreductase 1 (NQO1) promoter. The ARE is a key regulatory region in the NQO1 gene promoter activated in response to oxidative stress[69]. The positive control, elesclomol, induced ROS production in HeLa cells[35], but WHN-11 did not (Supplementary Fig. 1b). Consistent with the NQO1 promoter activity in HeLa cells, WHN-11 treatment did not alter NQO1 mRNA levels in HCC1937 cells (Supplementary Fig. 1c). The ROS scavenger, *N*-acetyl-L-cysteine (NAC) did not alter the toxicity of WHN-11, but did reverse the cytotoxic effects of elesclomol and artemisinin that act through ROS production (Supplementary Fig. 1d). Taken together, these data suggested that WHN-11 showed anti-cancer toxicity but did not induce significant ROS formation in cancer cells.

WHN-11 treatment perturbs protein homeostasis in HCC1937 cells

To understand the mode of action of WHN-11, we conducted an unbiased global analysis of the proteome of WHN-11 versus vehicle-treated HCC1937 cells by mass spectrometry[53]. A total of 3,629 unique proteins were identified, of which 51 proteins were significantly upregulated (> twofold) and 84 significantly downregulated (< -twofold) in WHN-11-treated cells versus the vehicle treatment (Supplementary Fig. 2). Some significantly upregulated proteins included the death-associated protein 1 (DAP), ubiquitin-like modifier-activating enzyme (ATG7), interferon-stimulated gene 15 (ISG15), ubiquitin specific peptidase 24 (USP24) and E3 ubiquitin-protein ligase (HERC2). Significantly downregulated proteins included the cytochrome c oxidase assembly factor 7 (COA7), vacuolar protein sorting-associated protein 37B (VPS37B), Ras-related protein Rap-2B (RAP2B), growth arrest and DNA damage-inducible proteins-interacting protein 1 (GADD45GIP1) and cyclin-dependent kinase 4 (CDK4; Supplementary Material).

Twelve of the upregulated proteins were identified only in the WHN-11-treated samples. Among these were ubiquitin carboxyl-terminal hydrolase 24 (USP24), profilin-2 (PFN2), ADP-ribosylation factor 6 (ARF6) and mas-related genes (MRG/MORF4L)-binding protein (MRGBP) (Supplementary Material). In addition, 18 downregulated proteins were detected only in DMSO-treated cells. These included the ATP-binding cassette sub-family B member 10 (ABCB10), nuclear factor 1 B-type (NF1B), growth arrest and DNA damage-inducible proteins-interacting protein 1 (GADD45GIP1) and tumour necrosis factor alpha-induced protein 2 (TNFAIP2; Supplementary Material).

Gene set enrichment analysis[53,54] showed that WHN-11 altered gene sets associated with development and morphogenesis, transmembrane transport, cell cycle, serine/threonine kinase activity and Wnt signalling (Fig. 3a, Supplementary Material). Multiple gene sets involved in protein catabolism, ubiquitination, cellular responses to starvation and protein targeting to the lysosome were identified as significantly enriched (either

a

TERM	SIZE	ES	NES	NOM P-VAL
GOBP_EMBRYONIC_DIGIT_MORPHOGENESIS	17	0.71	1.9	0.003
HP_ABNORMALITY_OF_ALKALINE_PHOSPHATASE_LEVEL	26	0.63	1.9	0.009
HP_PATHOLOGIC_FRACTURE	22	0.62	1.83	0.003
HP_MYOTONIA	16	0.68	1.81	0
GOMF_SECONDARY_ACTIVE_TRANSMEMBRANE_TRANSPORTER_ACTIVITY	36	0.53	1.72	0.006
GOBP_RESPONSE_TO_AMINO_ACID_STARVATION	**22**	**0.59**	**1.72**	**0.017**
GOBP_ORGANIC_ACID_TRANSMEMBRANE_TRANSPORT	39	0.51	1.71	0
GOBP_AMINO_ACID_TRANSMEMBRANE_TRANSPORT	21	0.59	1.69	0.015
HP_ABNORMALITY_OF_TIBIA_MORPHOLOGY	23	0.56	1.67	0.016
GOBP_REGULATION_OF_SYNAPSE_ASSEMBLY	18	0.6	1.66	0.015
GOBP_PROTEIN_TARGETING_TO_LYSOSOME	**16**	**0.62**	**1.65**	**0.024**
GOMF_ORGANIC_ANION_TRANSMEMBRANE_TRANSPORTER_ACTIVITY	39	0.48	1.64	0.003
GOBP_L_AMINO_ACID_TRANSPORT	19	0.59	1.63	0.014
HP_ADDUCTED_THUMB	37	0.49	1.6	0.013
GOBP_PROTEIN_LOCALIZATION_TO_LYSOSOME	**22**	**0.56**	**1.6**	**0.03**
GOBP_RESPONSE_TO_STARVATION	**72**	**0.43**	**1.6**	**0.004**
GOBP_PROTEIN_TARGETING_TO_VACUOLE	**23**	**0.55**	**1.59**	**0.019**
GOMF_SYMPORTER_ACTIVITY	19	0.57	1.59	0.037
HP_IMMUNOLOGIC_HYPERSENSITIVITY	51	0.46	1.59	0.01
GOBP_CELLULAR_RESPONSE_TO_STARVATION	**58**	**0.43**	**1.58**	**0.012**
GOBP_KIDNEY_EPITHELIUM_DEVELOPMENT	29	-0.7	-1.94	0
GOBP_REGULATION_OF_CANONICAL_WNT_SIGNALING_PATHWAY	79	-0.6	-1.9	0
GOBP_CONNECTIVE_TISSUE_DEVELOPMENT	61	-0.6	-1.88	0
GOBP_REGULATION_OF_PROTEASOMAL_UBIQUITIN_DEPENDENT_PROTEIN_CATABOLIC_PROCESS	**67**	**-0.6**	**-1.87**	**0**
GOBP_REGULATION_OF_WNT_SIGNALING_PATHWAY	104	-0.6	-1.87	0
GOBP_NEGATIVE_REGULATION_OF_PROTEASOMAL_PROTEIN_CATABOLIC_PROCESS	**27**	**-0.7**	**-1.86**	**0.001**
GOBP_POSITIVE_REGULATION_OF_WNT_SIGNALING_PATHWAY	49	-0.6	-1.85	0
GOMF_CYCLIN_DEPENDENT_PROTEIN_SERINE_THREONINE_KINASE_REGULATOR_ACTIVITY	15	-0.8	-1.84	0
GOBP_REGULATION_OF_CELL_CYCLE_CHECKPOINT	15	-0.8	-1.84	0
GOBP_RENAL_TUBULE_DEVELOPMENT	15	-0.8	-1.83	0.002
GOBP_NEGATIVE_REGULATION_OF_PROTEASOMAL_UBIQUITIN_DEPENDENT_PROTEIN_CATABOLIC_PROCESS	**23**	**-0.7**	**-1.83**	**0.003**
GOMF_PROMOTER_SPECIFIC_CHROMATIN_BINDING	36	-0.6	-1.83	0.001
GOBP_CHROMOSOME_SEGREGATION	164	-0.5	-1.81	0
GOBP_NEGATIVE_REGULATION_OF_WNT_SIGNALING_PATHWAY	47	-0.6	-1.81	0
GOBP_NEGATIVE_REGULATION_OF_EPITHELIAL_CELL_PROLIFERATION	30	-0.7	-1.8	0
GOBP_CANONICAL_WNT_SIGNALING_PATHWAY	84	-0.5	-1.8	0.001
GOBP_PROTEIN_K48_LINKED_UBIQUITINATION	**29**	**-0.7**	**-1.8**	**0**
GOCC_ORGANELLAR_RIBOSOME	57	-0.6	-1.79	0
GOBP_RIBONUCLEOSIDE_TRIPHOSPHATE_BIOSYNTHETIC_PROCESS	21	-0.7	-1.78	0.003
GOBP_P_BODY_ASSEMBLY	15	-0.7	-1.78	0.002

b

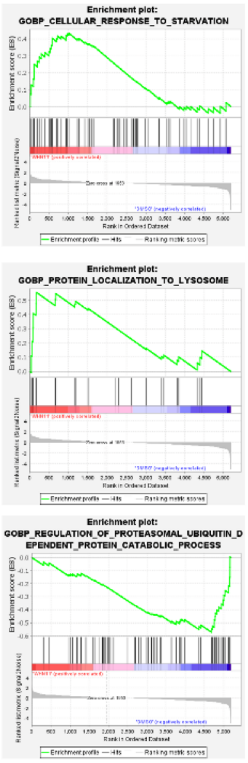

c

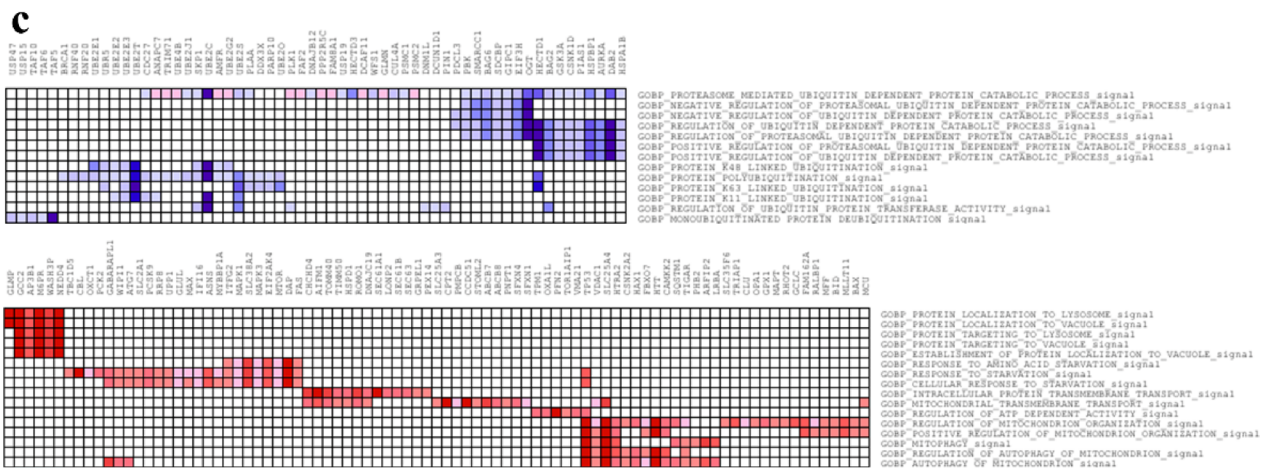

Fig. 3. WHN-11 induces changes in cellular proteome associated with protein turnover. Gene set enrichment analysis (GSEA) of proteomic changes associated with WHN-11 treatment. (**a**) Significantly positively (top 20) and negatively (top 20) enriched gene sets in WHN-11 versus DMSO treated cells. (**b**) Gene set enrichment plots of genes associated with response to starvation, targeting to lysosome and protein catabolism. (**c**) Leading edge analysis identifying gene clusters associated with protein catabolism, ubiquitination, lysosome, mitochondrion, and cellular starvation. Red shading indicates gene sets or genes enriched in WHN-11 lysates compared to the DMSO lysates, while blue shading indicates genes enriched in the DMSO treated lysates relative to WHN-11. The volcano plot linked to these data are provided in the Supplementary Figures.

positively or negatively) upon WHN-11 treatment (Fig. 3a–c). Consistent with our biological assays, we did not detect significant enrichment of genes associated with ROS production.

The global proteomic analysis suggested WHN-11 affected proteostasis, including ubiquitination and proteasomal degradation. Both processes occur during cellular stress induced by the unfolded protein response (UPR) and/or the heat shock response (HSR)[70]. Artemisinin treatment induced protein ubiquitination in malaria cultures[71]. The induction of protein ubiquitination by WHN-11 in HCC1937 cells was analysed in the absence or presence of the proteasome inhibitor MG132. Immunofluorescence (IF) staining showed ubiquitinated proteins in the cytoplasm, decreasing dose dependently upon WHN-11 treatment. This suggested that WHN-11 increased proteasome activity (Figs. 4a, b). We observed a significant accumulation of ubiquitinated protein aggregates

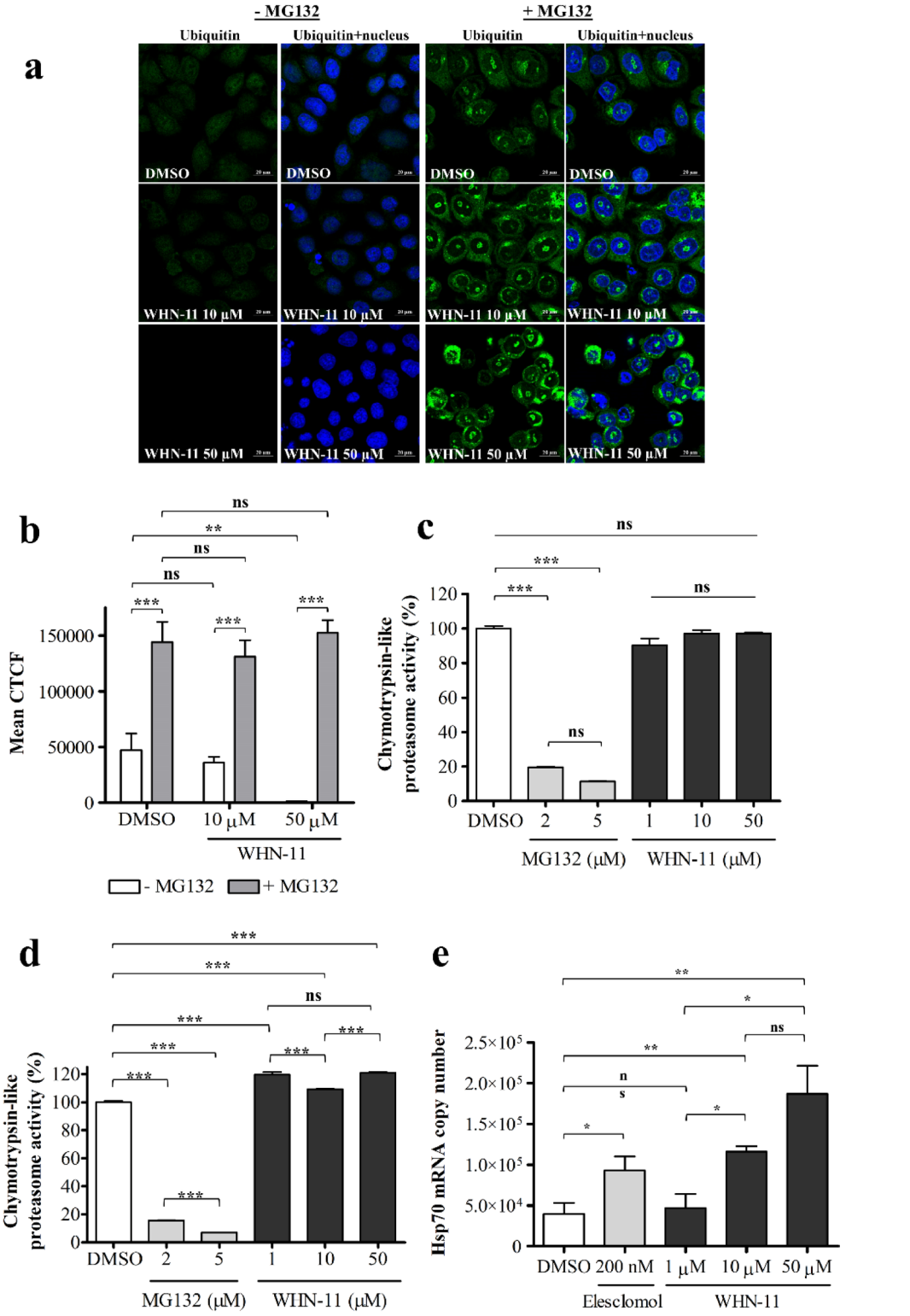

Fig. 4. WHN-11 promotes protein ubiquitination and turnover in HCC1937 cells. (**a**) Confocal analysis staining of ubiquitin in untreated cells or cells treated with 2 µM MG132. Representative images shown (n = 3). (**b**) Mean of the Corrected Total Cell Fluorescence (CTFC). Data represent averages ± SD (n = 3), where significance levels are indicated as ** $p < 0.01$, *** $p < 0.001$ and ns–not significant using two-way ANOVA with Bonferroni post-test. (**c**) Direct chymotrypsin-like proteasome inhibition activity assay in cell lysates. (**d**) Proteasome activity after overnight pre-treatment of live cells prior to lysate preparation. Data shown are averages ± SEM (n = 3), where significance levels are indicated as *** $p < 0.001$ and ns—not significant using One-way ANOVA with Bonferroni's multiple comparison test. (**e**) Quantitative analysis of the mRNA copy number of Hsp70 in treated HCC1937 cells. Data shown are averages ± SEM (n = 3), where significance levels are defined as * $p < 0.05$, ** $p < 0.01$ and ns—not significant using a two-tailed student´s t-test.

localized at the periphery and within the nucleus of cells co-treated with MG132 and WHN-11 (Fig. 4a). More so, higher concentrations of WHN-11 increased cytoplasmic protein aggregates (Fig. 4a). Artemisinin disrupts protein homeostasis and inhibits the malarial proteasome[71]. To test WHN-11 inhibited human proteasomes, we assessed the ability of the WHN-11 to directly inhibit the proteasome in whole cell lysates. MG132 treatment inhibited the chymotrypsin-like activity of the proteasome in a dose-dependent manner. WHN-11 did not significantly alter the proteasome activity compared to the vehicle treatment (Fig. 4c). However, when cells were treated overnight prior to assessment of proteasome activity in lysates, WHN-11 significantly increased proteasome activity (Fig. 4d). In combination experiments, WHN-11 and MG132 exhibited a strong synergistic relationship (Table 1, Supplementary Fig. 3). Changes due to proteostatic stress were indicated by a significant increase in the stress-responsive Hsp70 mRNA levels in WHN-11-treated cells (Fig. 4e). These data suggested that WHN-11 does not directly inhibit the proteasome, but promotes protein turnover via the proteasome by a distinct mechanism[72].

WHN-11 induced autophagy in cancer cells

WHN-11-induced apoptosis and proteasome-independent regulation of protein turnover. This suggest that autophagy may play a role as an alternative degradation pathway in the mechanism of action of WHN-11. This was supported by the gene set enrichment analysis which identified responses to starvation and protein targeting to the lysosome (Fig. 3). We previously observed the formation of vesicle-like structures in WHN-11 treated cells (data not shown), which indicated possible sites of early endosomal or autophagic vesicles, lipid, or other acidic vesicles[73,74]. Formation of acidic vesicular organelles (AVOs) in HCC1937 cells treated with WHN-11 was assessed using acridine orange (AO) dye and confocal microscopy. We used Hanks' Balanced Salt Solution (HBSS) as an autophagy inducer. WHN-11 significantly increased the formation of cytoplasmic AVOs (Figs. 5a, b) and the number of cells with AVOs compared to the vehicle treatment (white arrows, Fig. 5c). Although these observations suggested possible WHN-11-induced formation of autophagosomes, other vesicle-like structures (yellow arrows) not coinciding with AVOs were visible (Fig. 5a). Using Nile Red dye, treatment with WHN-11 and HBSS showed enlarged lipid droplets (LDs) in the cytosol and near the nuclear membranes (Fig. 5d). LDs are specialized compartments for fatty acid products after lysosomal degradation[75] and are formed autophagy[76].

We subsequently established that WHN-11 activated autophagy, as indicated bythe lipidation of LC3B-I. This effect was enhanced by co-treatment with chloroquine (CQ) (Fig. 6a). While treatment at 1 and 4 h show LC3B-1 lipidation comparable to the 0-h baseline, longer treatment significantly increased autophagy (Fig. 6b). WHN-11, like the controls HBSS and colchicine, significantly decreased the association between GFP-Bcl2 and Beclin1-FLAG in transiently transfected HEK293T cells relative to the vehicle control (Fig. 6c). This indicated autophagy induction[77]. WHN-11 treatment enhanced autophagic flux in HeLa cells as evidenced by the formation of autophagic vesicles. We stably transfected HeLa cells with an mCherry-EGFP-LC3 plasmid that is a marker for autophagy induction. Cells treated with WHN-11 had increased yellow puncta. This yellow vesicles arise from the overlap of green-EGFP and red-mCherry signals indicating autophagosome formation[78] (Supplementary Fig. 4). WHN-11 also showed strong synergy with the autophagy inducers rapamycin, tunicamycin and the autophagy inhibitor CQ and moderate synergism with autophagy inhibitor 3-methyladenine (3-MA) (Table 1).

WHN-11 induces mitochondrial dysfunction

WHN-11 induced both autophagy (as indicated by LC3B-I lipidation) and apoptosis (as indicated by caspase-3 cleavage) only after a prolonged exposure of 16 h (Fig. 6b). This suggested that other molecular events may precede cell death. The mitochondrial Bcl2 family of proteins drive apoptosis[79]. Prior to mitochondrial-induced (intrinsic) apoptosis, mitochondrial membrane potential $\Delta\Psi m$ changes, ATP levels drop and Bcl2 levels change[80]. WHN-11 significantly decreased the expression of anti-apoptotic Bcl-xL like the positive control KRIBB-11 (Fig. 7a). This confirms the apoptotic response to WHN-11 and linked its mechanism of action to the mitochondrion. Consistent with these observations, WHN-11 reduced cellular ATP in a dose-dependent manner (Fig. 7b). The mitochondrial membrane potential $\Delta\Psi m$ enhances the transfer of protons between the matrix and intermembrane space (IMS) during ATP synthesis[81]. A loss in $\Delta\Psi m$ causes mitochondrial outer membrane permeabilization (MOMP), a non-reversible apoptotic stage involving the release of essential proteins within the mitochondrial IMS[82]. Changes in the $\Delta\Psi m$ were determined using the membrane permeable JC-1 dye[83]. WHN-11 mediated a significant loss in $\Delta\Psi m$ (Fig. 7c), consistent with the positive control carbonyl cyanide *m*-chlorophenylhydrazone (CCCP). WHN-11 dose-dependently suppressed Bcl-xL protein levels compared to the vehicle treatment (Fig. 7d). Furthermore, WHN-11 treatment enhanced a reticular network of TRAP1 staining, which showed a pattern consistent with mitochondrial localisation. Notably, WHN-11 did not alter TRAP1

Compound	Mechanism of action	Average CI* when combined with WHN-11	Relationship
MG132	Proteasome inhibitor	0.20	Strong synergism
Chloroquine	Inhibits lysosome acidification	0.19	Strong synergism
Rapamycin	mTOR inhibitor	0.34	Strong synergism
Tunicamycin	Glycosylation inhibitor	0.38	Strong synergism
3-Methyladenine	PI3K inhibitor	0.58	Moderate synergism

Table 1. WHN-11 synergizes with inducers or activators of autophagy and proteostatic stress. *Average combination index (CI) where half the population of cells are affected by the co-treatment with the compounds (Fa = 0.5).

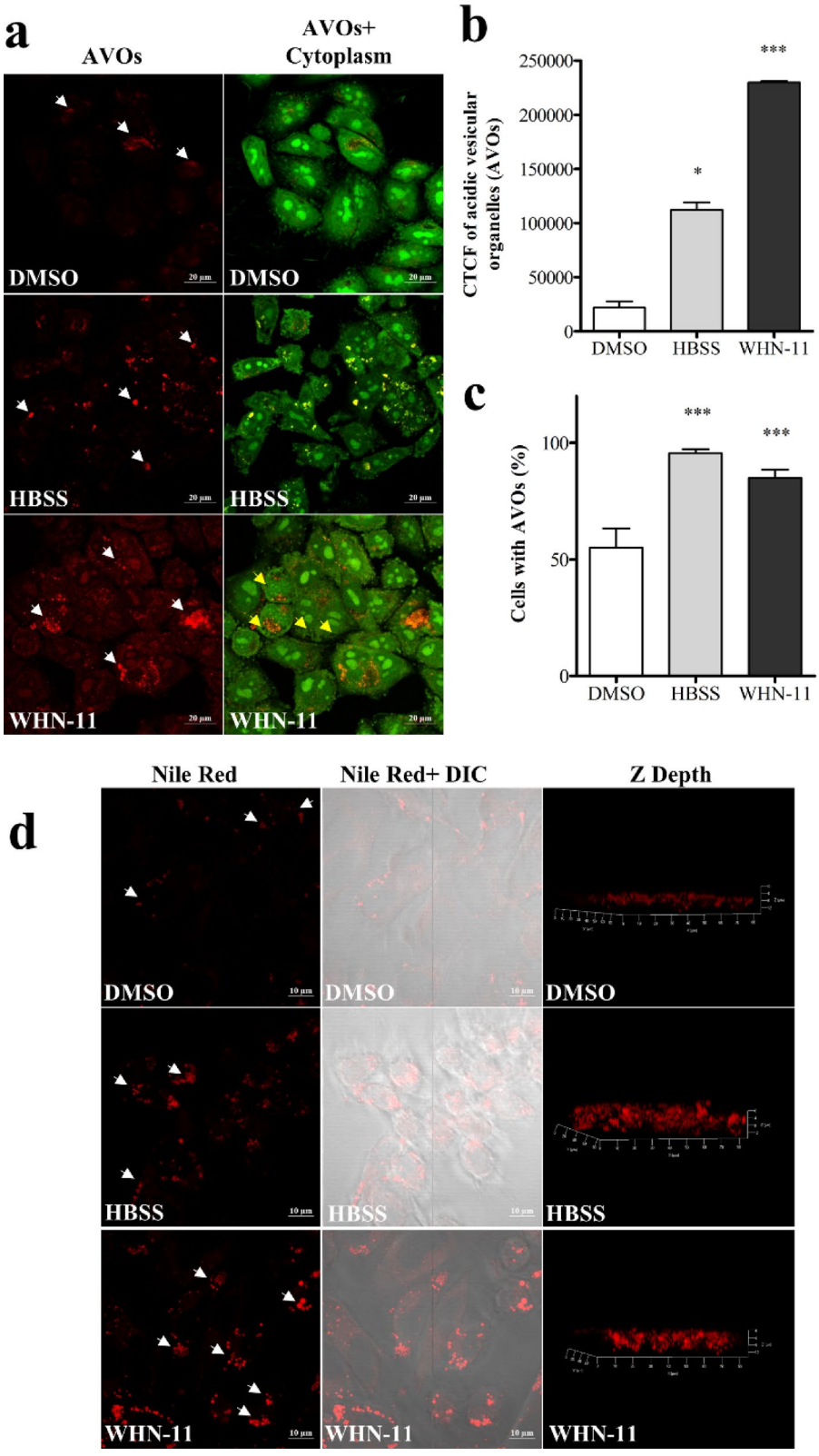

Fig. 5. WHN-11 promotes formation of autophagic vesicles and lipid droplets in HCC1937 cells. (**a**) Acidic vesicular organelles (AVOs, white arrows) detected with acridine orange dye in cells treated for 4 h with 0.1% DMSO, 10 µM WHN-11 or Hanks' Balanced Salt Solution (HBSS). Yellow arrows indicate unstained vesicles. Quantitation of (**b**) fluorescence intensity of AVOs and (**c**) number of cells with AVOs. Data represent averages ± SEM (n = 3), where significance levels are indicated as * $p < 0.05$, ** $p < 0.01$ and *** $p < 0.001$ using a One-way ANOVA. (**d**) Lipid droplets (white arrows) stained with Nile Red dye in cells treated for 4 h with 0.1% DMSO, HBSS or 10 µM WHN-11. Z depth panel shows 3D z-stack of equivalent depth. Representative images shown (n = 3).

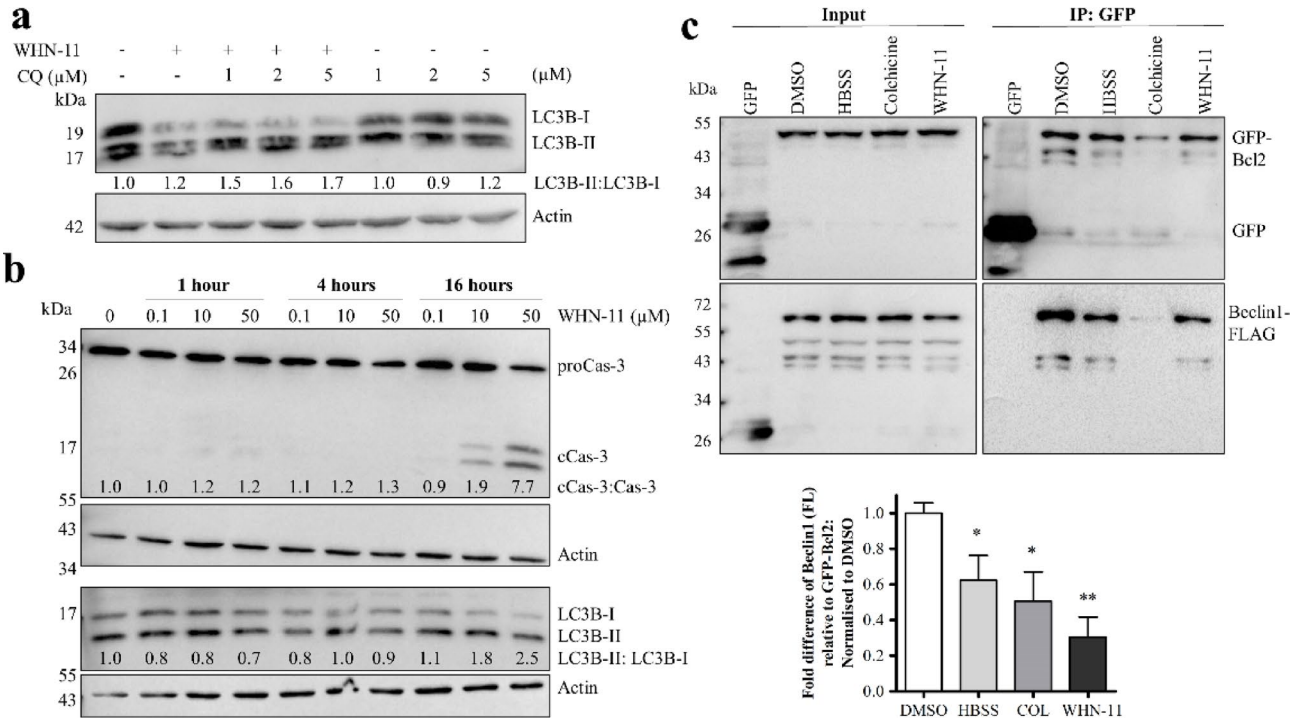

Fig. 6. Activation of apoptotic and autophagic signalling pathways in WHN-11-treated HCC1937 cells. (**a**) Western blot analysis of LC3B lipidation in cells treated overnight with 10 μM WHN-11 and for 4 h with 2 μM chloroquine (CQ). Actin was used as a loading control. Ratios indicated are normalized to the untreated control. Representative blot shown (n = 2). See supplementary blot figure F2 for full length blots. (**b**) Time-dependent treatment of cells with 0.1% DMSO or WHN-11 for caspase-3 and LC3B activation. Actin was used as a loading control. Ratios of LC3B-II: LC3B-I and cCas-3:Cas-3 are normalized to the untreated control. Representative blot shown (n = 2). See supplementary blot figure F3 for full length blots. (**c**) Immunoprecipitation of GFP or GFP-Bcl2 complexes in lysates (input) for HEK293T cells transfected with pLV-eGFP (untreated control) or GFP-Bcl2 and Beclin1-FLAG for 48 h and treated for 3 h with 0.1% DMSO, Hanks' Balanced Salt Solution (HBSS), 5 μM colchicine or 10 μM WHN-11. Representative blots shown. Analysis of the average fold difference ± SEM (n = 3) of Beclin1-FLAG levels in immunoprecipitates relative to GFP-Bcl2 and normalized to DMSO treatment (taken as 1), where significance levels are indicated as * $p < 0.05$ and ** $p < 0.01$ using a two-tailed student's t-test. See supplementary blot figure F4 for full length blots.

staining intensity, but did induce distinct morphological changes in mitochondria. Vehicle treated cells had an elongated tubular mitochondria network (Figs. 7di and ii). In contrast, WHN-11-treated cells had mitochondria which appeared fragmented, an indication of mitochondrial stress or dysfunction[84].

To confirm the mitotoxic role of WHN-11, we assessed WHN-11 toxicity in cells grown in either glucose- or galactose-containing medium. In high glucose concentrations, cancer cells produce ATP via glycolysis and suppress oxidative phosphorylation, a process called the Crabtree effect. The Crabtree effect is reversed by replacing glucose with galactose to promote ATP production via oxidative phosphorylation (OXPHOS) in the mitochondria[85]. Increased sensitivity of cells to compounds in the presence of galactose indicates mitotoxicity[86]. Galactose significantly increased the toxicity of WHN-11 (GAL-IC_{50} = 0.19 ± 0.07 μM, GLU-IC_{50} = 0.74 ± 0.40 μM) in HCC1937 cells. In contrast, the toxicity of artemisinin was not significantly different (GAL-IC_{50} = 218.00 ± 80.69 μM, GLU-IC_{50} = 389.33 ± 92.70 μM; Table 2). This suggested that WHN-11 targets the mitochondria to induce toxicity. Mitochondrial dysfunction upon WHN-11 treatment may also explain the inability to detect significant ROS production (Supplementary Fig. 1).

Discussion

Studies on novel therapies and the identification of alternative cellular targets to address the lack of standardised treatment for TNBC are ongoing[87]. The anti-cancer properties of artemisinins are well studied[21–27,29,31–35]. Many artemisinin derivatives including artemisinin hybrids connected to different pharmacophores[88], artemisinin dimers and others show activity against tumour cells[89–92]. The amino-artemisinin WHN-11 is structurally unique in incorporating a nitrogen atom attached directly to C-10 which is attached by a piperazine linker to a *p*-trifluoromethylaryl urea group (Fig. 1). WHN-11 exhibited the highest cytotoxicity (IC_{50} 0.19 ± 1.52 μM) among the amino-artemisinins against TNBC cell lines compared to the parent compound artemisinin (202.90 ± 1.30 μM). To date, the mechanisms of action of artemisinin and its derivatives is still a topic of significant debate. The predominant view of the mechanism of action of artemisinins is the induction of ROS in cancer cells[21,29,32]. Indeed, artemisinin[93], DHA[67], artemether[94] and artesunate[36] (Fig. 1) used to treat malaria,

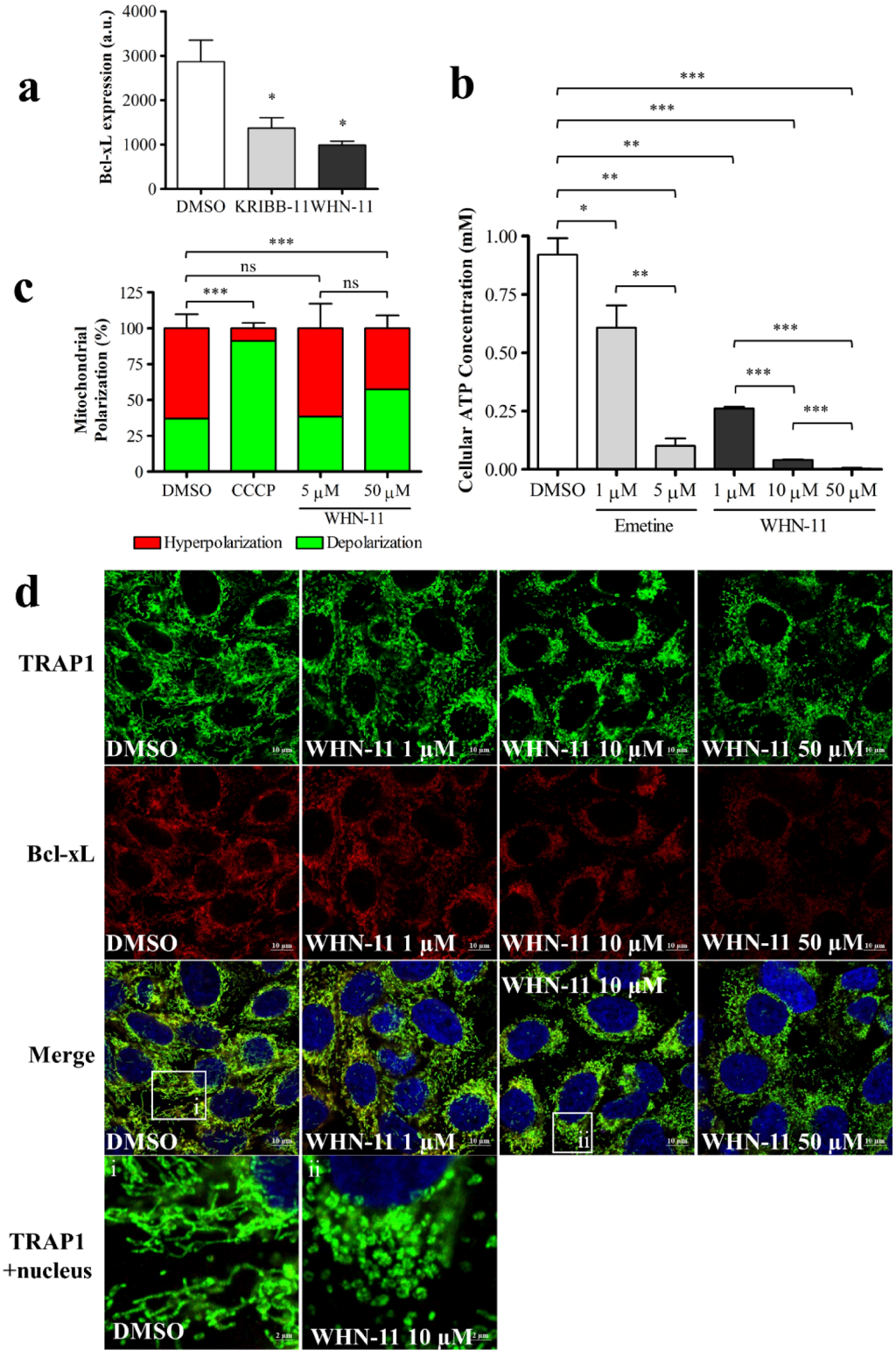

Fig. 7. WHN-11 disrupts mitochondrial function. (**a**) Analysis of Bcl-xL expression in treated HCC1937 cells overnight. Data indicate the mean fluorescence intensity ± SEM (n = 3), where significance levels are indicated as * $p < 0.05$ using a two-tailed student's t-test. (**b**) Cellular ATP levels quantified in treated cells. Data shown are averages ± SEM (n = 3), where significance levels are indicated as * $p < 0.05$, ** $p < 0.01$ and *** $p < 0.001$ using a two-tailed student's t-test. (**c**) Mitochondrial membrane potential (ΔΨm) measured by JC-1 staining in treated HCC1937 cells. Data shown are averages ± SEM (n = 3) of the relative percentage ratio of red to green fluorescence, where significance levels are indicated as ** $p < 0.01$, *** $p < 0.001$ and ns–not significant using a two-tailed student's t-test. (**d**) Confocal analysis of the mitochondrial morphology indicated by TRAP1 and Bcl-xL staining in treated HCC1937 cells. Representative images shown (n = 2).

Compound	IC_{50} (μM) ± SD (n = 3)	
	Glucose	Galactose
Artemisinin	389.33 ± 92.70	218.00 ± 80.69 (ns)
WHN-11	0.74 ± 0.40	0.19 ± 0.07 (*)

Table 2. IC_{50} values of artemisinins in HCC1937 cells in glucose- and galactose-containing medium. Statistical significance of IC_{50} values in + galactose samples relative to + glucose samples was determined using a two-tailed student's t-test, where significance levels are indicated as * $p < 0.05$ and ns–not significant.

also show toxicity to range of cancer cells through production of ROS. However, artemisinin is specific for ROS-induction by malaria parasite and yeast mitochondria, and not mammalian mitochondria[95]. Furthermore, artemisinin and its derivatives can induce cell death independent of ROS generation[96]. Artemisinin derivatives have been linked to perturbations in protein homeostasis. DHA-mediated cell death in malaria parasites involves protein damage and proteasome inhibition. This activates ER-stress related cell death[71]. In contrast to the effects of DHA in the malaria parasite[71], WHN-11 did not directly inhibit the proteasome. WHN-11 rather promoted a modest but significant increase in proteosome activity coinciding with increased ubiquitinated protein turnover. Overall this is consistent with increased autophagy.

Therefore, it is likely that artemisinin derivatives can induce cell death via multiple mechanisms depending on the context. For WHN-11, we have no evidence of significant ROS induction using a range of biological assays, including those previously used to demonstrate ROS production by artemisinins. While this may be due to technical reasons in detection of ROS, it may also be explained by the observed mitochondrial dysfunction. Many artemisinins induce apoptotic cell death through mitochondrial dysfunction in cancer cells that is not exclusively associated with ROS production[46,47]. WHN-11 resulted in mitochondrial fission, MOMP, loss of ATP production and down-regulation of the anti-apoptotic mitochondrial protein Bcl-xL culminating in apoptosis. The toxicity of WHN-11 was potentiated by reliance of cells on OXPHOS for ATP production. Taken together, this suggested that mitochondrial defects induced by WHN-11 were a main cause of toxicity. Mitochondrial fission is a known stress response linked to apoptosis, and both cell stress and apoptosis were induced by WHN-11 treatment. The reduced Bcl-xL levels induced by treatment with WHN-11 must culminate in release of Bax from inhibitory Bcl-xL-Bax complexes, allowing free Bax to promote mitochondrial fission linked to apoptosis[97,98]. Indeed, artesunate induced Bax-mediated apoptosis in HepG2 cells, and this was also independent of ROS production[47].

The role autophagy induction by WHN-11 as a cell death mechanism is less clear. Other artemisinins also induce autophagy and resistance to artemisinin therapy is linked to autophagy in the malaria parasite[99]. Like WHN-11, DHA activated major apoptotic and autophagy-related proteins, and suppressed the interaction between Bcl2 and Beclin1, promoting cell death in KKU-213 cholangiocarcinoma cells[100]. In normal cells, autophagy is a pro-survival response which is upregulated in response to stress, particularly starvation, to provide nutrients for cell survival. In cancer cells, autophagy is linked to both tumour killing and tumour survival, although the mechanisms are not well defined. In the case of WHN-11, it is likely that autophagy is activated as a response to mitochondrial dysfunction to circumvent or prevent apoptosis. The lipid accumulation observed upon WHN-11 treatment can arise due to a lack of OXPHOS from mitochondrial defects which subsequently triggers autophagy[101]. Mitochondria and MOMP are important in autophagy activation[102], although this process is usually in response to oxidative stress and associated with ROS production[103]. In the case of WHN-11 however, in the absence of any substantive evidence supporting ROS production, we assume that ROS-independent changes to the mitochondria may trigger autophagy and subsequently cell death by apoptosis. There is a growing appreciation of the role of autophagy modulators, both activators and inhibitors, in potentiating the anti-cancer activity of several chemotherapeutic agents for clinical benefit[104]. Therefore, the next steps require an evaluation of drug combinations of WHN-11 and structurally related amino-artemisinin derivatives with known modulators of autophagy like temsirolimus or everolimus in the drive to develop these compounds as viable chemotherapeutic options, in particular for treatment of TNBC.

Conclusion

We report the promising anti-cancer activity of a novel amino-artemisinin derivative WHN-11 against multiple cell lines, including the aggressive TNBC subtype. Unlike most other artemisinin derivatives, WHN-11 anti-cancer activity was independent of substantive ROS production. Rather, WHN-11 altered cellular protein homeostasis pathways to induce mitochondrial fission and dysfunction. This deprived the cell of ATP, activating autophagy and subsequent cell death by apoptosis. The anti-cancer effect of WHN-11 was synergistic with inducers of autophagy, suggesting that future combination treatment with modulators of autophagy will have therapeutic potential. This study reports early-stage preclinical findings, with subsequent analysis needed to validate the mechanism of action of WHN-11 in additional cancer cell line models, including HCC70 and HCT116 cell lines and the non-cancerous MCF-12A line. These data will better characterize the therapeutic potential of WHN-11 and its specificity. Future preclinical studies will incorporate animal models to optimize formulation of WHN-11, assess its efficacy, and evaluate its safety profile, paving the way for potential future clinical application.

Data availability

The datasets used and/or analysed during the current study are available from the corresponding author on reasonable request.

Received: 23 October 2024; Accepted: 2 June 2025
Published online: 01 July 2025

References

1. Hsu, E. Reflections on the "discovery" of the antimalarial qinghao. *Br J Clin Pharmacol* **61**, 666–670. https://doi.org/10.1111/j.1365-2125.2006.02673.x (2006).
2. Ho, W. E., Peh, H. Y., Chan, T. K. & Wong, W. S. F. Artemisinins: Pharmacological actions beyond anti-malarial. *Pharmacol Ther* **142**, 126–139. https://doi.org/10.1016/j.pharmthera.2013.12.001 (2014).
3. Wu, Y., Tang, W. & Zuo, J. Development of artemisinin drugs in the treatment of autoimmune diseases. *Sci Bull (Beijing)* **61**, 37–41. https://doi.org/10.1007/S11434-015-0975-9 (2016).
4. Kim, S. K., Choe, J. Y. & Park, K. Y. Anti-inflammatory effect of artemisinin on uric acid-induced NLRP3 inflammasome activation through blocking interaction between NLRP3 and NEK7. *Biochem Biophys Res Commun* **517**, 338–345. https://doi.org/10.1016/J.BBRC.2019.07.087 (2019).
5. Cheong, D. H. J., Tan, D. W. S., Wong, F. W. S. & Tran, T. Anti-malarial drug, artemisinin and its derivatives for the treatment of respiratory diseases. *Pharmacol Res* **158**, 104901. https://doi.org/10.1016/J.PHRS.2020.104901 (2020).
6. Loo, C. S. N. et al. Artemisinin and its derivatives in treating protozoan infections beyond malaria. *Pharmacol Res* **117**, 192–217. https://doi.org/10.1016/J.PHRS.2016.11.012 (2017).
7. Efferth, T. et al. The antiviral activities of artemisinin and artesunate. *Clin Infect Dis* **47**, 804–811. https://doi.org/10.1086/591195 (2008).
8. Liu, X. et al. Biological activities of artemisinin derivatives beyond malaria. *Curr Top Med Chem* **19**, 205–222. https://doi.org/10.2174/1568026619666190122144217 (2019).
9. Meng, Y. et al. Recent pharmacological advances in the repurposing of artemisinin drugs. *Med Res Rev* **41**, 3156–3181. https://doi.org/10.1002/MED.21837 (2021).
10. Li, D., Zhang, J. & Zhao, X. Mechanisms and molecular targets of artemisinin in cancer treatment. *Cancer Invest* **39**, 675–684. https://doi.org/10.1080/07357907.2021.1954190 (2021).
11. Wong, Y. K. et al. Artemisinin as an anticancer drug: Recent advances in target profiling and mechanisms of action. *Med Res Rev* **37**, 1492–1517. https://doi.org/10.1002/med.21446 (2017).
12. Slezakova, S. & Ruda-Kucerova, J. Anticancer activity of artemisinin and its derivatives. *Anticancer Res* **37**, 5995–6003. https://doi.org/10.21873/anticanres.12046 (2017).
13. Konstat-Korzenny, E., Ascencio-Aragón, J. A., Niezen-Lugo, S. & Vázquez-López, R. Artemisinin and its synthetic derivatives as a possible therapy for cancer. *Med. Sci.* https://doi.org/10.3390/MEDSCI6010019 (2018).
14. Zhang, Y. et al. Antitumor research on artemisinin and its bioactive derivatives. *Nat Prod Bioprospect* **8**, 303–319. https://doi.org/10.1007/s13659-018-0162-1 (2018).
15. Kiani, B. H. et al. Artemisinin and its derivatives: a promising cancer therapy. *Mol Biol Rep* **47**, 6321–6336. https://doi.org/10.1007/S11033-020-05669-Z (2020).
16. Xu, C., Zhang, H., Mu, L. & Yang, X. Artemisinins as anticancer drugs: novel therapeutic approaches, molecular mechanisms, and clinical trials. *Front Pharmacol* **11**, 529881. https://doi.org/10.3389/FPHAR.2020.529881/BIBTEX (2020).
17. Mancuso, R. I., Foglio, M. A. & Olalla Saad, S. T. Artemisinin-type drugs for the treatment of hematological malignancies. *Cancer Chemother Pharmacol* **87**, 1–22. https://doi.org/10.1007/S00280-020-04170-5/FIGURES/1 (2021).
18. Khanal, P. Antimalarial and anticancer properties of artesunate and other artemisinins: Current development. *Monatsh Chem* **152**, 387–400. https://doi.org/10.1007/S00706-021-02759-X/FIGURES/12 (2021).
19. Augustin, Y., Staines, H. M. & Krishna, S. Artemisinins as a novel anti-cancer therapy: Targeting a global cancer pandemic through drug repurposing. *Pharmacol Ther* https://doi.org/10.1016/J.PHARMTHERA.2020.107706 (2020).
20. Yang, X. et al. Progress on the study of the anticancer effects of artesunate. *Oncol. Lett.* https://doi.org/10.3892/OL.2021.13011 (2021).
21. Gravett, A. M. et al. In vitro study of the anti-cancer effects of artemisone alone or in combination with other chemotherapeutic agents. *Cancer Chemother Pharmacol* **67**, 569–577. https://doi.org/10.1007/S00280-010-1355-4 (2011).
22. Das, A. Anticancer effect of antimalarial artemisinin compounds. *Ann. Med. Health Sci. Res.* **5**, 93. https://doi.org/10.4103/2141-9248.153609 (2015).
23. Van Huijsduijnen, R. H. et al. Anticancer properties of distinct antimalarial drug classes. *PLoS ONE* **8**, e82962. https://doi.org/10.1371/JOURNAL.PONE.0082962 (2013).
24. Dwivedi, A. et al. In vitro anti-cancer effects of artemisone nano-vesicular formulations on melanoma cells. *Nanomedicine* **11**, 2041–2050. https://doi.org/10.1016/J.NANO.2015.07.010 (2015).
25. Hegedűs, C. et al. Redox control of cancer cell destruction. *Redox Biol* **16**, 59. https://doi.org/10.1016/J.REDOX.2018.01.015 (2018).
26. Efferth, T. Cancer combination therapies with artemisinin-type drugs. *Biochem Pharmacol* **139**, 56–70. https://doi.org/10.1016/J.BCP.2017.03.019 (2017).
27. Kumar, M. S. et al. Combination therapies of artemisinin and its derivatives as a viable approach for future cancer treatment. *Curr. Pharm. Des.* **25**, 3323–3338. https://doi.org/10.2174/1381612825666190902155957 (2019).
28. Wong, H. N. et al. Anti-melanoma activities of artemisone and prenylated amino-artemisinins in combination with known anticancer drugs. *Front Pharmacol* https://doi.org/10.3389/fphar.2020.558894 (2020).
29. Hornsveld, M. & Dansen, T. B. The hallmarks of cancer from a redox perspective. *Antioxid Redox Signal* **25**, 300–325. https://doi.org/10.1089/ARS.2015.6580 (2016).
30. Dixon, S. J. & Stockwell, B. R. The role of iron and reactive oxygen species in cell death. *Nat Chem Biol* **10**, 9–17. https://doi.org/10.1038/nchembio.1416 (2014).
31. Sun, Y. et al. ROS systems are a new integrated network for sensing homeostasis and alarming stresses in organelle metabolic processes. *Redox Biol.* https://doi.org/10.1016/J.REDOX.2020.101696 (2020).
32. Haynes, R. K. et al. Interactions between artemisinins and other antimalarial drugs in relation to the cofactor model–a unifying proposal for drug action. *ChemMedChem* **7**, 2204–2226. https://doi.org/10.1002/cmdc.201200383 (2012).
33. Haynes, R. K. et al. Facile oxidation of leucomethylene blue and dihydroflavins by artemisinins: relationship with flavoenzyme function and antimalarial mechanism of action. *ChemMedChem* **5**, 1282–1299. https://doi.org/10.1002/CMDC.201000225 (2010).
34. Haynes, R. K. et al. Reactions of antimalarial peroxides with each of leucomethylene blue and dihydroflavins: flavin reductase and the cofactor model exemplified. *ChemMedChem* **6**, 279–291. https://doi.org/10.1002/CMDC.201000508 (2011).
35. Nagai, M. et al. The oncology drug elesclomol selectively transports copper to the mitochondria to induce oxidative stress in cancer cells. *Free Radic Biol Med* **52**, 2142–2150. https://doi.org/10.1016/j.freeradbiomed.2012.03.017 (2012).

36. Qin, G. et al. Artesunate induces apoptosis via a ROS-independent and Bax-mediated intrinsic pathway in HepG2 cells. *Exp Cell Res* **336**, 308–317. https://doi.org/10.1016/j.yexcr.2015.07.004 (2015).
37. Greenshields, A. L., Fernando, W. & Hoskin, D. W. The anti-malarial drug artesunate causes cell cycle arrest and apoptosis of triple-negative MDA-MB-468 and HER2-enriched SK-BR-3 breast cancer cells. *Exp Mol Pathol* **107**, 10–22. https://doi.org/10.1016/j.yexmp.2019.01.006 (2019).
38. Dent, R. et al. Triple-negative breast cancer: Clinical features and patterns of recurrence. *Clin. Cancer Res.* **13**, 4429–4434. https://doi.org/10.1158/1078-0432.CCR-06-3045 (2007).
39. Anders, C. & Carey, L. A. Understanding and treating triple-negative breast cancer. *Oncology* **22**, 1233–1239 (2008).
40. Maniam, S. & Maniam, S. Small molecules targeting programmed cell death in breast cancer cells. *Int. J. Mol. Sci.* https://doi.org/10.3390/IJMS22189722 (2021).
41. Ryu, W. J. & Sohn, J. H. Molecular targets and promising therapeutics of triple-negative breast cancer. *Pharmaceuticals (Basel)* https://doi.org/10.3390/PH14101008 (2021).
42. Nath, A. et al. Molecular targets and therapeutics in chemoresistance of triple-negative breast cancer. *Med Oncol* **39**, 14–14. https://doi.org/10.1007/S12032-021-01610-X (2021).
43. Haynes, R. K. et al. Highly antimalaria-active artemisinin derivatives: Biological activity does not correlate with chemical reactivity. *Angewandte Chemie - International Edition* **43**, 1381–1385. https://doi.org/10.1002/anie.200352343 (2004).
44. Haynes, R. K. et al. Artemisone–A highly active antimalarial drug of the artemisinin class. *Angewandte Chemie – Int. Edition* **45**, 2082–2088. https://doi.org/10.1002/anie.200503071 (2006).
45. Coertzen, D. et al. Artemisone and artemiside are potent panreactive antimalarial agents that also synergize redox imbalance in plasmodium falciparum transmissible gametocyte stages. *Antimicrob Agents Chemother* https://doi.org/10.1128/AAC.02214-17 (2018).
46. Wong, H. N. et al. Optimal 10-aminoartemisinins with potent transmission-blocking capabilities for new artemisinin combination therapies-activities against blood stage P. falciparum including PfKI3 C580Y mutants and liver stage P. berghei Parasites. *Front Chem* **7**, 1–16. https://doi.org/10.3389/fchem.2019.00901 (2020).
47. Watson, D. J. et al. Toward new transmission-blocking combination therapies: Pharmacokinetics of 10-amino-artemisinins and 11-aza-artemisinin and comparison with dihydroartemisinin and artemether. *Antimicrob Agents Chemother* https://doi.org/10.1128/AAC.00990-21 (2021).
48. Wu, Y. et al. Facile preparation of N-glycosylated 10-piperazinyl artemisinin derivatives and evaluation of their antimalarial and cytotoxic activities. *Molecules* https://doi.org/10.3390/MOLECULES23071713 (2018).
49. de la Mare, J.-A. et al. Assessment of potential anti-cancer stem cell activity of marine algal compounds using an in vitro mammosphere assay. *Cancer Cell Int* **13**, 39. https://doi.org/10.1186/1475-2867-13-39 (2013).
50. Laemmli, U. K. Cleavage of structural proteins during the assembly of the head of bacteriophage T4. *Nature* **227**, 680–685. https://doi.org/10.1038/227680a0 (1970).
51. Turriziani, B. et al. On-beads digestion in conjunction with data-dependent mass spectrometry: A shortcut to quantitative and dynamic interaction proteomics. *Biology (Basel)* **3**, 320–332. https://doi.org/10.3390/biology3020320 (2014).
52. Mootha, V. K. et al. PGC-1α-responsive genes involved in oxidative phosphorylation are coordinately downregulated in human diabetes. *Nat. Genet.* **34**(3), 267–273. https://doi.org/10.1038/ng1180 (2003).
53. Subramanian, A. et al. Gene set enrichment analysis: A knowledge-based approach for interpreting genome-wide expression profiles. *Proce. Natl. Acad. Sci.* https://doi.org/10.1073/pnas.0506580102 (2005).
54. Smiley, S. T. et al. Intracellular heterogeneity in mitochondrial membrane potentials revealed by a J-aggregate-forming lipophilic cation JC-1. *Proc Natl Acad Sci U S A* **88**, 3671–3675. https://doi.org/10.1073/pnas.88.9.3671 (1991).
55. Chou, T. C. & Talalay, P. Analysis of combined drug effects: a new look at a very old problem. *Trends Pharmacol Sci* **4**, 450–454. https://doi.org/10.1016/0165-6147(83)90490-X (1983).
56. Chou T, Martin N (2005) CompuSyn for drug combinations: PC software and user's guide: a computer program for quantitation of synergism and antagonism in drug combinations,. ComboSyn, Paramus, NJ
57. Chan, W. C. et al. Evaluation and optimization of synthetic routes from dihydroartemisinin to the alkylamino-artemisinins artemiside and artemisone: A test of N-glycosylation methodologies on a lipophilic peroxide. *Tetrahedron* **74**, 5156–5171. https://doi.org/10.1016/J.TET.2018.04.027 (2018).
58. Zhou, X. et al. Artemisinin derivatives stimulate DR5-specific TRAIL-induced apoptosis by regulating wildtype P53. *Cancers (Basel)* **12**, 1–15. https://doi.org/10.3390/CANCERS12092514 (2020).
59. Yu, Z., Pestell, T. G., Lisanti, M. P. & Pestell, R. G. Cancer stem cells. *Int J Biochem Cell Biol* **44**, 2144–2151. https://doi.org/10.1016/j.biocel.2012.08.022 (2012).
60. Vidal, S. J. et al. Targeting cancer stem cells to suppress acquired chemotherapy resistance. *Oncogene* **33**, 4451–4463 (2014).
61. Franken, N. A. P. et al. Clonogenic assay of cells in vitro. *Nat Protoc* **1**, 2315–2319. https://doi.org/10.1038/nprot.2006.339 (2006).
62. Wang, N. et al. 5-FU inhibits migration and invasion of CRC cells through PI3K/AKT pathway regulated by MARCH1. *Cell Biol Int* **45**, 368. https://doi.org/10.1002/CBIN.11493 (2020).
63. Yoo, K., Yun, H. H., Jung, S. Y. & Lee, J. H. KRIBB11 induces apoptosis in A172 glioblastoma cells via MULE-dependent degradation of MCL-1. *Molecules* https://doi.org/10.3390/MOLECULES26144165 (2021).
64. Chen, H., Li, L. Q. & Pan, D. Geldanamycin induces apoptosis in human gastric carcinomas by affecting multiple oncogenic kinases that have synergic effects with TNF-related apoptosis-inducing ligand. *Oncol Lett* **10**, 3732–3736. https://doi.org/10.3892/OL.2015.3807 (2015).
65. Luo, Y. et al. Dihydroartemisinin exposure impairs porcine ovarian granulosa cells by activating PERK-eIF2α-ATF4 through endoplasmic reticulum stress. *Toxicol Appl Pharmacol* https://doi.org/10.1016/J.TAAP.2020.115159 (2020).
66. Mancuso, R. I., Foglio, M. A. & Olalla Saad, S. T. Artemisinin-type drugs for the treatment of hematological malignancies. *Cancer Chemother Pharmacol* **87**, 1–22. https://doi.org/10.1007/S00280-020-04170-5/TABLES/6 (2021).
67. Poupel, F. et al. Dihydroartemisinin induces apoptosis in human bladder cancer cell lines through reactive oxygen species, mitochondrial membrane potential, and cytochrome C pathway. *Int J Prev Med* https://doi.org/10.4103/IJPVM.IJPVM_258_17 (2017).
68. Chen, W. et al. Artemisitene activates the Nrf2-dependent antioxidant response and protects against bleomycin-induced lung injury. *FASEB J.* **30**, 2500–2510. https://doi.org/10.1096/fj.201500109R (2016).
69. Dinkova-Kostova, A. T. & Talalay, P. NAD(P)H:quinone acceptor oxidoreductase 1 (NQO1), a multifunctional antioxidant enzyme and exceptionally versatile cytoprotector. *Arch Biochem Biophys* **501**, 116. https://doi.org/10.1016/J.ABB.2010.03.019 (2010).
70. Higuchi-Sanabria, R. et al. A futile battle? protein quality control and the stress of aging. *Dev Cell* **44**, 139–163 (2018).
71. Bridgford, J. L. et al. Artemisinin kills malaria parasites by damaging proteins and inhibiting the proteasome. *Nat. Commun.* **9**, 1–9. https://doi.org/10.1038/s41467-018-06221-1 (2018).
72. Ciechanover, A. Proteolysis: From the lysosome to ubiquitin and the proteasome. *Nat. Rev. Mol. Cell Biol.* **6**, 79–86 (2005).
73. Casey, J. R., Grinstein, S. & Orlowski, J. Sensors and regulators of intracellular pH. *Nat. Rev Mol. Cell Biol.* **11**, 50–61 (2010).
74. Katariina Lähdesmäki, O. H., Ollila, S., Koivuniemi, A., Kovanen, P. T. & Hyvönen, M. T. Membrane simulations mimicking acidic pH reveal increased thickness and negative curvature in a bilayer consisting of lysophosphatidylcholines and free fatty acids. *Biochimica et Biophysica Acta (BBA)–Biomembranes* **1798**(5), 938–946. https://doi.org/10.1016/j.bbamem.2010.01.020 (2010).

75. Jaishy, B. & Abel, E. D. Thematic review series: Lipotoxicity: Many roads to cell dysfunction and cell death lipids, lysosomes, and autophagy. *J. Lipid Res.* **57**, 1619–1635 (2016).
76. Shibata, M. et al. The MAP1-LC3 conjugation system is involved in lipid droplet formation. *Biochem Biophys Res Commun* **382**, 419–423. https://doi.org/10.1016/j.bbrc.2009.03.039 (2009).
77. Rubinstein, A. D. & Kimchi, A. Life in the balance–A mechanistic view of the crosstalk between autophagy and apoptosis. *J. Cell Sci.* **125**, 5259–5268 (2012).
78. Yoshii, S. R. & Mizushima, N. Monitoring and measuring autophagy. *Int. J. Mol. Sci.* **18**, 1–13. https://doi.org/10.3390/ijms18091865 (2017).
79. Tzifi, F. et al. The role of BCL2 family of apoptosis regulator proteins in acute and chronic leukemias. *Adv. Hematol.* **2012**, 524308. https://doi.org/10.1155/2012/524308 (2012).
80. Wang, C. & Youle, R. J. The role of mitochondria in apoptosis. *Annu. Rev. Genet.* **43**, 95–118. https://doi.org/10.1146/annurev-genet-102108-134850 (2009).
81. Tait, S. W. G. & Green, D. R. Mitochondria and cell death: Outer membrane permeabilization and beyond. *Nat. Rev. Mol. Cell Biol.* **11**, 621–632 (2010).
82. Chipuk, J. E., Bouchier-Hayes, L. & Green, D. R. Mitochondrial outer membrane permeabilization during apoptosis: The innocent bystander scenario. *Cell Death Differ.* **13**, 1396–1402 (2006).
83. Sivandzade, F., Bhalerao, A. & Cucullo, L. Analysis of the mitochondrial membrane potential using the cationic JC-1 dye as a sensitive fluorescent probe. *Bio-Protoc.* https://doi.org/10.21769/BioProtoc.3128 (2019).
84. Butler, E. K. et al. The mitochondrial chaperone protein TRAP1 mitigates α-synuclein toxicity. *PLoS Genet.* **8**, e1002488. https://doi.org/10.1371/JOURNAL.PGEN.1002488 (2012).
85. Mot, A. I., Liddell, J. R., White, A. R. & Crouch, P. J. Circumventing the crabtree effect: a method to induce lactate consumption and increase oxidative phosphorylation in cell culture. *Int. J. Biochem. Cell Biol.* **79**, 128–138. https://doi.org/10.1016/j.biocel.2016.08.029 (2016).
86. Marroquin, L. D. et al. Circumventing the Crabtree effect: replacing media glucose with galactose increases susceptibility of HepG2 cells to mitochondrial toxicants. *Toxicol Sci.* **97**, 539–547. https://doi.org/10.1093/TOXSCI/KFM052 (2007).
87. Lyons, T. G. Targeted therapies for triple-negative breast cancer. *Curr. Treat Options Oncol.* **20**, 82. https://doi.org/10.1007/s11864-019-0682-x (2019).
88. Wang, L.-L.L. et al. Design and synthesis of novel artemisinin derivatives with potent activities against colorectal cancer in vitro and in vivo. *Eur. J. Med. Chem.* **182**, 111665. https://doi.org/10.1016/j.ejmech.2019.111665 (2019).
89. Chen, J., Zhang, L. & Hao, M. Effect of artemisinin on proliferation and apoptosis-related protein expression in vivo and in vitro. *Saudi J. Biol. Sci.* **25**, 1488–1493. https://doi.org/10.1016/j.sjbs.2018.04.003 (2018).
90. Zhu, Y. et al. Novel dihydroartemisinin dimer containing nitrogen atoms inhibits growth of endometrial cancer cells and may correlate with increasing intracellular peroxynitrite. *Sci Rep* **9**, 1–14. https://doi.org/10.1038/s41598-019-52108-6 (2019).
91. Wang, S. & Sasaki, T. Synthesis of artemisinin dimers using the Ugi reaction and their in vitro efficacy on breast cancer cells.. *Bioorg. Med. Chem. Lett.* **23**, 4424–4427. https://doi.org/10.1016/j.bmcl.2013.05.057 (2013).
92. Zhang, N. et al. Synthesis of novel ring-contracted artemisinin dimers with potent anticancer activities. *Eur. J. Med. Chem.* **150**, 829–840. https://doi.org/10.1016/j.ejmech.2018.03.010 (2018).
93. Jia, J. et al. Artemisinin inhibits gallbladder cancer cell lines through triggering cell cycle arrest and apoptosis. *Mol. Med. Rep.* **13**, 4461–4468. https://doi.org/10.3892/mmr.2016.5073 (2016).
94. Alcântara, D. D. F. Á. et al. In vitro evaluation of the cytotoxic and genotoxic effects of artemether, an antimalarial drug in a gastric cancer cell line (PG100). *J. Appl. Toxicol.* **33**, 151–156. https://doi.org/10.1002/jat.1734 (2013).
95. Wang, J. et al. Artemisinin directly targets malarial mitochondria through its specific mitochondrial activation. *PLoS ONE* **5**, e9582. https://doi.org/10.1371/journal.pone.0009582 (2010).
96. Gotsbacher, M. P. et al. Reverse chemical proteomics identifies an unanticipated human target of the antimalarial artesunate. *ACS Chem Biol* **14**, 63A6-643. https://doi.org/10.1021/acschembio.8b01004 (2019).
97. Billen, L. P. et al. Bcl-XL inhibits membrane permeabilization by competing with Bax. *PLoS Biol* **6**, e147. https://doi.org/10.1371/journal.pbio.0060147 (2008).
98. Frank, S. et al. The role of dynamin-related protein 1, a mediator of mitochondrial fission, in apoptosis. *Dev Cell* **1**, 515–525. https://doi.org/10.1016/s1534-5807(01)00055-7 (2001).
99. Ray A, Mathur M, Choubey D, et al (2022) Autophagy underlies the proteostasis mechanisms of artemisinin resistance in P. falciparum Malaria. mBio 13:. https://doi.org/10.1128/MBIO.00630-22
100. Thongchot, S. et al. Dihydroartemisinin induces apoptosis and autophagy-dependent cell death in cholangiocarcinoma through a DAPK1-BECLIN1 pathway. *Mol Carcinog* **57**, 1735–1750. https://doi.org/10.1002/mc.22893 (2018).
101. Bosc, C. et al. Autophagy regulates fatty acid availability for oxidative phosphorylation through mitochondria-endoplasmic reticulum contact sites. *Nature Commun.* **11**, 1. https://doi.org/10.1038/s41467-020-17882-2 (2020).
102. Lyamzaev, K. G. et al. Induction of autophagy by depolarization of mitochondria. *Autophagy* **14**, 921–924. https://doi.org/10.1080/15548627.2018.1436937 (2018).
103. Roca-Agujetas, V. et al. Recent insights into the mitochondrial role in autophagy and its regulation by oxidative stress. *Oxid. Med. Cell. Longev.* **2019**, 3809308. https://doi.org/10.1155/2019/3809308 (2019).
104. Levy, J. M. M. & Thorburn, A. Targeting autophagy during cancer therapy to improve clinical outcomes. *Pharmacol. Ther.* **131**, 130. https://doi.org/10.1016/J.PHARMTHERA.2011.03.009 (2011).

Acknowledgements

We thank our colleagues Heinrich Hoppe, Demetra Mavri-Damelin, Sharon Prince, Anna-Mart Engelbrecht and Earl Prinsloo for providing reagents and conducting useful discussions.

Author contributions

Conceptualization, A.L.E, J.d.l.M, and D.K.; formal analysis, D.K, A.L.E, J.d.l.M; investigation, D.K, H.N.W and A.v.K; resources, R.K.H and A.v.K; data curation, D.K, A.v.K, and A.L.E; writing—original draft preparation, D.K, A.L.E. and R.K.H; writing—review and editing, J.d.l.M and A.v.K; visualization, D.K and A.L.E; supervision, A.L.E, J.d.l.M and R.K.H; project admin-istration, A.L.E; funding acquisition, A.L.E and R.K.H. All authors have read and agreed to the published version of the manuscript.

Funding

Organization of Women in Science for the Developing World (OWSD) and Swedish International Development Cooperation Agency (Sida),PhD Fellowship,the South African Medical Research Council (MRC) Flagship Project,MRC-RFA-UFSP-01–2013,National Research Foundation,90682,129262,98934,129135, 121914,90682 ,129262,98934,129135, 121914,90682,129262,98934,129135, 121914,South African Research Chairs Initiative

(SARChI) of the Department of Science and Innovation (DSI) and National Research Foundation (NRF) of South Africa,98566,Rhodes University, RGG-Edkins

Declarations

Competing interests
The authors declare no competing interests.

Additional information
Supplementary Information The online version contains supplementary material available at https://doi.org/10.1038/s41598-025-05284-7.

Correspondence and requests for materials should be addressed to A.L.E.

Reprints and permissions information is available at www.nature.com/reprints.

Publisher's note Springer Nature remains neutral with regard to jurisdictional claims in published maps and institutional affiliations.